

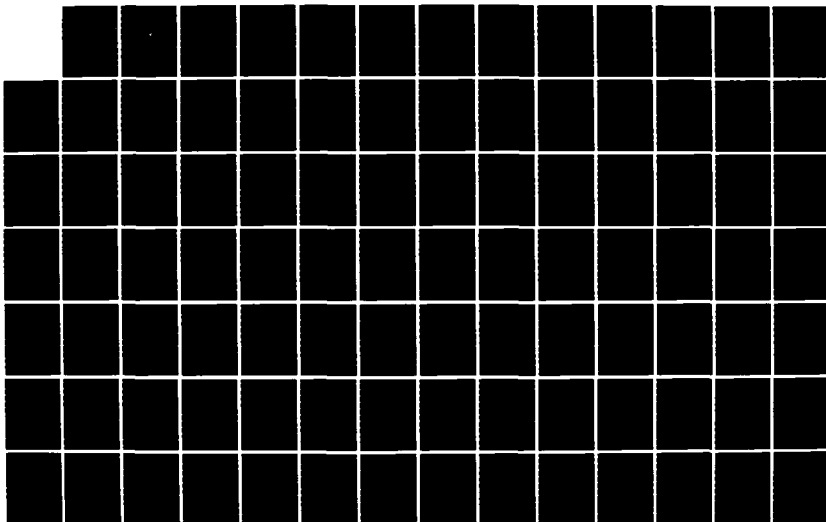
AD-A167 887

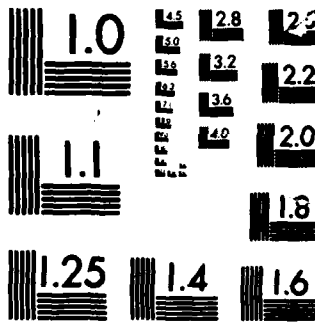
A PARAMETRIC STUDY OF ELASTIC RESPONSES OF
SUBMARINE-INSTALLED EQUIPMENT. (U) NAVAL POSTGRADUATE
SCHOOL MONTEREY CA S A WEINHARDT MAR 86

1/2

UNCLASSIFIED

F/G 13/10.1 NL





MICROCOM

CHART

2

AD-A167 807

NAVAL POSTGRADUATE SCHOOL

Monterey, California



DTIC
ELECTE
MAY 22 1986
S E D

THESIS

A PARAMETRIC STUDY OF ELASTIC RESPONSES
OF SUBMARINE-INSTALLED EQUIPMENT WHEN
SUBJECTED TO UNDEX END-ON LOADING

by

Stephen Allen Weinhardt
March 1986

Thesis Advisor:

Young S. Shin

Approved for public release; distribution is unlimited

DTIC FILE COPY

REPORT DOCUMENTATION PAGE

1a. REPORT SECURITY CLASSIFICATION UNCLASSIFIED		1b. RESTRICTIVE MARKINGS	
2a. SECURITY CLASSIFICATION AUTHORITY		3. DISTRIBUTION/AVAILABILITY OF REPORT Approved for public release; distribution is unlimited	
2b. DECLASSIFICATION/DOWNGRADING SCHEDULE		4. PERFORMING ORGANIZATION REPORT NUMBER(S)	
4. PERFORMING ORGANIZATION REPORT NUMBER(S)		5. MONITORING ORGANIZATION REPORT NUMBER(S)	
6a. NAME OF PERFORMING ORGANIZATION Naval Postgraduate School	6b. OFFICE SYMBOL (If applicable) 69	7a. NAME OF MONITORING ORGANIZATION Naval Postgraduate School	
6c. ADDRESS (City, State, and ZIP Code) Monterey, California 93943-5000		7b. ADDRESS (City, State, and ZIP Code) Monterey, California 93943-5000	
8a. NAME OF FUNDING/SPONSORING ORGANIZATION	8b. OFFICE SYMBOL (If applicable)	9. PROCUREMENT INSTRUMENT IDENTIFICATION NUMBER	
8c. ADDRESS (City, State, and ZIP Code)		10. SOURCE OF FUNDING NUMBERS	
		PROGRAM ELEMENT NO.	PROJECT NO.
		TASK NO.	WORK UNIT ACCESSION NO.
11. TITLE (Include Security Classification) A PARAMETRIC STUDY OF ELASTIC RESPONSES OF SUBMARINE-INSTALLED EQUIPMENT WHEN SUBJECTED TO UNDEX END-ON LOADING			
12. PERSONAL AUTHOR(S) Weinhardt, Stephen Allen			
13a. TYPE OF REPORT Master's Thesis	13b. TIME COVERED FROM TO	14. DATE OF REPORT (Year, Month, Day) 1986 March	15. PAGE COUNT 110
16. SUPPLEMENTARY NOTATION			
17. COSATI CODES		18. SUBJECT TERMS (Continue on reverse if necessary and identify by block number)	
FIELD	GROUP	ELSHOK	
	SUB-GROUP	End-On Load	
19. ABSTRACT (Continue on reverse if necessary and identify by block number)			
<p>Due to the lack of longitudinal stiffening along submarine hulls, they are inherently vulnerable to underwater explosions directly off the bow or stern. Accordion-like deformations of the hull are set into motion which could cause dynamic amplification in the transient response of attached substructures. In underwater shock acceptance tests of internal equipment, this interaction is created by exploding a charge in a fore and aft configuration with the submerged shock test vehicle (SSTV). With the increasing availability of large computers and the rapid development of numerical methods, several computer codes have been written to predict equipment response to underwater shocks. Using the ELSHOK (ELASTIC SHOCK) code, this investigation studies the effect of hull/substructure</p>			
20. DISTRIBUTION/AVAILABILITY OF ABSTRACT <input checked="" type="checkbox"/> UNCLASSIFIED/UNLIMITED <input type="checkbox"/> SAME AS RPT. <input type="checkbox"/> DTIC USERS		21. ABSTRACT SECURITY CLASSIFICATION Unclassified	
22a. NAME OF RESPONSIBLE INDIVIDUAL Professor Young S. Shin		22b. TELEPHONE (Include Area Code) (408) 646-2568	22c. OFFICE SYMBOL 69Sg

19. (Continued)

interaction on stiffened shell response at resonance following an end-on load. The transient response of the coupled shell/substructure system from tapered and conventional charges of equivalent impulse is examined in this study.

Accession For	
NTIS GRA&I	<input checked="" type="checkbox"/>
DTIC TAB	<input type="checkbox"/>
Unannounced	<input type="checkbox"/>
Justification	
By	
Distribution/	
Availability Codes	
Dist	Avail and/or Special
A-1	

Approved for public release; distribution is unlimited

A Parametric Study of Elastic Responses
of Submarine-Installed Equipment When
Subjected to UNDEX End-On Loading

by

Stephen Allen Weinhardt
Lieutenant Commander, United States Navy
B.S., Purdue University, 1975

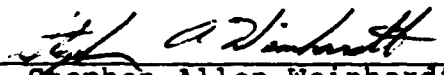
Submitted in partial fulfillment of the
requirements for the degree of

MASTER OF SCIENCE IN MECHANICAL ENGINEERING

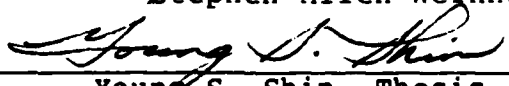
from the

NAVAL POSTGRADUATE SCHOOL
March 1986

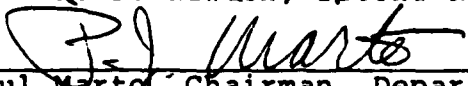
Author:



Stephen Allen Weinhardt

Approved by:


Young S. Shin, Thesis Advisor


R. E. Newton, Second Reader


Paul Marto, Chairman, Department of
Mechanical Engineering


John N. Dyer, Dean of Science and Engineering

ABSTRACT

Due to the lack of longitudinal stiffening along submarine hulls, they are inherently vulnerable to underwater explosions directly off the bow or stern. Accordion-like deformations of the hull are set into motion which could cause dynamic amplification in the transient response of attached substructures. In underwater shock acceptance tests of internal equipment, this interaction is created by exploding a charge in a fore and aft configuration with the submerged shock test vehicle (SSTV). With the increasing availability of large computers and the rapid development of numerical methods, several computer codes have been written to predict equipment response to underwater shocks. Using the ELSHOK (ELASTIC SHOCK) code, this investigation studies the effect of hull/substructure interaction on stiffened shell response at resonance following an end-on load. The transient response of the coupled shell/substructure system from tapered and conventional charges of equivalent impulse is examined in this study. *Replaces Friction shock loads.*

TABLE OF CONTENTS

I.	INTRODUCTION	12
A.	BACKGROUND	12
B.	PURPOSE FOR THIS INVESTIGATION	14
II.	EXPLOSIVE SHOCK RESPONSE USING ELSHOK	17
A.	GENERAL PRINCIPLES OF OPERATION	17
B.	ORGANIZATION AND OPERATION OF ELSHOK	18
	1. Phase I--Shell and Fluid Analysis	20
	2. Phase II--Substructure Analysis	22
	3. Phase III--Submerged Shock Response	22
	4. Phase IV--Plots of Velocity-Time Histories	24
III.	MODEL USED IN THE ANALYSIS	25
A.	SHELL MODEL	25
B.	SUBSTRUCTURE MODEL	31
IV.	ANALYSIS	34
A.	ANALYSIS PROCEDURE	34
V.	RESULTS	41
A.	VELOCITY-TIME HISTORY RESPONSE--EMPTY SHELL	41
B.	VELOCITY-TIME HISTORY RESPONSE-COUPLED SHELL/SUBSTRUCTURE SYSTEM	55
VI.	CONCLUSIONS	87
	LIST OF REFERENCES	91
	APPENDIX A: PROGRAM USED TO CONVERT PUSLOB PUNCH CARD FILES TO FORMAT ACCEPTABLE BY EASYPLOT	93

APPENDIX B: TYPICAL ELSHOK INPUT CODES--SHELL AND SUBSTRUCTURE	95
1. BOSOR4 INPUT DATA	95
2. ACESNID INPUT DATA	99
3. PIFLASH INPUT DATA100
4. SAPIV INPUT DATA101
5. PICRUST INPUT DATA103
6. USLOB INPUT DATA104
7. PUSLOB INPUT DATA106
INITIAL DISTRIBUTION LIST108

LIST OF TABLES

I.	MODES AND NATURAL FREQUENCIES OF SHELL	30
II.	FUNDAMENTAL FREQUENCIES OF DIAPHRAGM SUBSTRUCTURE	40
III.	MAXIMUM VELOCITY RESPONSE OF DIAPHRAGM SUBSTRUCTURE WITH VARYING THICKNESS (TAPER CHARGE)	56
IV.	MAXIMUM VELOCITY RESPONSE OF DIAPHRAGM SUBSTRUCTURE WITH VARYING THICKNESS (CONVENTIONAL CHARGE)	57

LIST OF FIGURES

1. Organization of the ELSHOK Computer Code	19
2. Nodal Patterns for Cylindrical Shells	21
3. Ring Stiffened Cylindrical Shell Used in Analysis	26
4. Typical Shell-Substructure Configuration	28
5. Finite Element Model of Diaphragm	33
6. Incident Pressure-Time History--Taper Charge	36
7. Incident Pressure-Time History--Conventional Charge	36
8. Velocity-Time History Response (Empty Shell)-- FWD Endplate Center	42
9. Velocity-Time History Response (Empty Shell)-- Frame Zero	43
10. Velocity-Time History Response (Empty Shell)-- Frame Five	44
11. Velocity-Time History Response (Empty Shell)-- Frame Nine	45
12. Velocity-Time History Response (Empty Shell)-- Frame Thirteen	46
13. Velocity-Time History Response (Empty Shell)-- Frame Eighteen	47
14. Velocity-Time History Response (Empty Shell)-- Frame Twenty-Three	48
15. Velocity-Time History Response (Empty Shell)-- Frame Twenty-Seven	49
16. Velocity-Time History Response (Empty Shell)-- Frame Thirty-Two	50
17. Velocity-Time History Response (Empty Shell)-- Frame Thirty-Six	51

18.	Velocity-Time History Response (Empty Shell)-- Frame Forty	52
19.	Velocity-Time History Response (Empty Shell)-- Frame Forty-Five	53
20.	Velocity-Time History Response (Empty Shell)-- AFT Endplate Center	54
21.	Diaphragm Maximum Velocity vs. Normalized Frequency	58
22.	Two Degree of Freedom System	59
23.	2-DOF System First Modal Frequency vs. Stiffness Ratio For Various Mass Ratios	60
24.	Energy Exchange Between Shell and Diaphragm (Taper Charge)	63
25.	Energy Exchange Between Shell and Diaphragm (Conventional Charge)	64
26.	Velocity-Time History Response (Resonant Case)--FWD Endplate Center	65
27.	Velocity-Time History Response (Resonant Case)--Frame Zero	66
28.	Velocity-Time History Response (Resonant Case)--Frame Five	67
29.	Velocity-Time History Response (Resonant Case)--Frame Nine	68
30.	Velocity-Time History Response (Resonant Case)--Diaphragm Center	69
31.	Velocity-Time History Response (Resonant Case)--Frame Thirteen	70
32.	Velocity-Time History Response (Resonant Case)--Frame Eighteen	71
33.	Velocity-Time History Response (Resonant Case)--Frame Twenty-Three	72
34.	Velocity-Time History Response (Resonant Case)--Frame Twenty-Seven	73

35.	Velocity-Time History Response (Resonant Case)--Frame Thirty-Two	74
36.	Velocity-Time History Response (Resonant Case)--Frame Thirty-Six	75
37.	Velocity-Time History Response (Resonant Case)--Frame Forty	76
38.	Velocity-Time History Response (Resonant Case)--Frame Forty-Five	77
39.	Velocity-Time History Response (Resonant Case)--AFT Endplate Center	78
40.	Comparison of Empty vs. Resonant Shell Response (Taper Charge)--Forward Endplate Center	80
41.	Comparison of Empty vs. Resonant Shell Response (Taper Charge)--Frame Nine	81
42.	Comparison of Empty vs. Resonant Shell Response (Taper Charge)--AFT Endplate Center	82
43.	Comparison of Empty vs. Resonant Shell Response (Conventional Charge)--Forward Endplate Center	83
44.	Comparison of Empty vs. Resonant Shell Response (Conventional Charge)--Frame Nine	84
45.	Comparison of Empty vs. Resonant Shell Response (Conventional Charge)--AFT Endplate Center	85

ACKNOWLEDGEMENT

I would like to express my deep appreciation to Professor Young S. Shin for his patience and support during the course of this thesis. The thorough technical guidance from Dr. David Ranlet of Weidlinger Associates greatly assisted in the formulation and execution of this study. Special thanks to Professor Robert Newton for his detailed review of this paper.

I. INTRODUCTION

A. BACKGROUND

Submarines are inherently vulnerable to explosions detonated directly off the bow or stern. While they have adequate protection against side loads with transverse bulkheads and frames, there is little longitudinal protection along the hull. As a result of this, they are susceptible to accordion-like deformations of the hull upon impact from end-on loads. It is possible that the frequency of the hull motions could excite internal equipment into resonance thereby causing unacceptable damage. This investigation examines the coupled elastic response of a shell/substructure system when subjected to an end-on underwater explosion (UNDEX) as the mass and stiffness of the internal substructure is varied.

The current specifications for conducting underwater shock tests on submarine-installed equipment are contained in MIL-S-901D [Ref. 1]. This document specifies the explosive charge weight and geometry of the test, as well as the mounting and orientation of the equipment being tested within the submerged shock test vehicle (SSTV). The SSTV is nothing more than a ring-stiffened cylindrical shell with circular endplates designed to simulate the hull motions

created by an underwater shock. Recognizing the potential for unacceptable damage to hull mounted equipment from an end-on load, the specification requires the first of four UNDEX's to be performed in a fore and aft configuration. The suitability of an equipment design or installation is evaluated according to its ability to function as intended during and after each shock impulse. Equipment tests of this nature are quite expensive and require a great deal of preparation. It is desirable for the designer to have some idea of what the transient response of the hull and equipment will be prior to the actual UNDEX.

The development of analytical methods and computer codes for the analysis of the reaction of submerged structures to underwater explosions has enabled the engineer to simulate the shock response of submarines and equipment with increasing accuracy. Finite-element/finite difference methods allow for the analysis of structure and fluid responses, and the work of Geers [Ref. 2] provides a means to incorporate fluid-structure interaction effects. Several computer codes currently exist which utilize these principles to analyze installed equipment response to shock waves. One of them is the ELSHOK (ELASTIC SHOCK) code developed by Weidlinger Associates, under the sponsorship of the Defense Nuclear Agency (DNA) and the Office of Naval Research (ONR). This code was developed to investigate

modern submarine underwater explosive shock response in conjunction with a testing program using small to large scale models and shaped or tapered explosive charges. The accuracy of ELSHOK has been validated in several highly controlled tests, notably the 1983 low level explosive test of an SSN 668 class submarine. The code was made available to the Naval Postgraduate School by the DNA with support from Weidlinger Associates. It was first used at the school by LT Mark Welch, USN, in his study comparing the shock response predictions of ELSHOK with those obtained using the Dynamic Design Analysis Method (DDAM) [Ref. 3].

B. PURPOSE FOR THIS INVESTIGATION

An explosive detonated underwater exerts a great amount of pressure on the surrounding fluid. The water is actually compressed by the force of the explosion causing a shock wave to form at the point of detonation which propagates in a roughly spherical shape at the speed of sound in water. When the pressure pulse impinges on a submarine, dynamic responses result in the hull from the fluid-structure interaction. The submarine experiences translational motion away from the point of impact. The velocity of this motion is of particular interest to a designer of submarines or weapons.

In an explosion with a side-on aspect with the submarine, the shock wave hits the hull in the middle before

it hits the ends due to its spherical shape. This causes the middle to bow away from the point of impact while the ends remain initially fixed. The resulting motion is called "whipping" as the hull bends back and forth about the middle. With an explosion off the bow or stern, the shock wave hits the submarine as a plane wave due to the small cross-sectional area at the point of impact. Since the force of the shock wave is axisymmetric about the centerline of the submarine, no whipping motion is induced in the hull. The inertial forces are transmitted down the hull until they reach the stern. The stern reacts violently to the combined inertial forces resulting from the explosion as well as the reflected pressure pulses from the water displaced by the translational motion of the submarine. After the initial transient response, the hull settles into an "accordion mode" about the middle where the motion of the bow opposes that of the stern.

The purpose of this investigation is to examine the shell/substructure interaction when subjected to UNDEX end-on loading using the ELSHOK code. The hull used in this study is a ring-stiffened cylindrical shell with endplates similar in shape to those used as SSTV's. The internal equipment or substructure is a diaphragm attached to the shell whose thickness is increased in order to study how the mass ratio between substructure and shell affects the

coupled transient response. The dynamic amplification of the response of the substructure at resonance is examined for both taper and conventional charges of equivalent impulse.

II. EXPLOSIVE SHOCK RESPONSE USING ELSHOK

A. GENERAL PRINCIPLES OF OPERATION

The ELSHOK computer code consists of a family of programs developed to calculate the transient response of a submerged, ring-stiffened shell of revolution of finite length to an underwater shock wave emanating from an explosive source located at an arbitrary point away from the structure [Ref. 4]. The shell is assumed to be linearly elastic, with or without internal substructures, and the surrounding fluid is treated as an infinite acoustic medium. Component modal analysis is employed in all phases of the calculations. The complete structural system is considered to consist of the ring-stiffened shell and any attached substructures. The vibration modes of each component are calculated separately, and the equations of motion for the entire system are obtained by enforcing compatibility of deformation at the points of attachment. The free-free modes of the empty ring-stiffened shell and the fixed-base modes of each individual substructure are coupled through the use of dynamic boundary conditions [Refs. 5, 6]. This eliminates the need to calculate the combined modes and natural frequencies of the entire system as well as the requirement for a combined system stiffness matrix.

The structure-fluid interaction is approximated in ELSHOK using the Doubly Asymptotic Approximation (DAA) methods of Geers [Ref. 2], expressed in terms of functions which are orthogonal over the wet surface of the submerged shell. By matching exact pressure-velocity relations at zero and infinite frequencies, the elements of the matrices in the resulting DAA are obtained. In transient problems, the DAA yields exact solutions at early and late times providing a smooth transition between these two limits. By accounting for the effects of the fluid with quantities defined solely on the wet surface of the shell, the DAA essentially uncouples the fluid field from the structural field.

B. ORGANIZATION AND OPERATION OF ELSHOK

As stated previously, the ELSHOK code contains a group of computer programs which are utilized in order to obtain velocity-time histories for various locations in the shell-substructure system. The programs, in order of execution, are:

- 1) BOSOR4--structural analyzer for shell [Ref. 7]
- 2) ACESNID--virtual mass processor
- 3) PIFLASH--shell-fluid processor
- 4) SAPIV--structural analyzer for substructure [Ref. 8]
- 5) PICRUST--substructure processor
- 6) USLOB--time integration processor

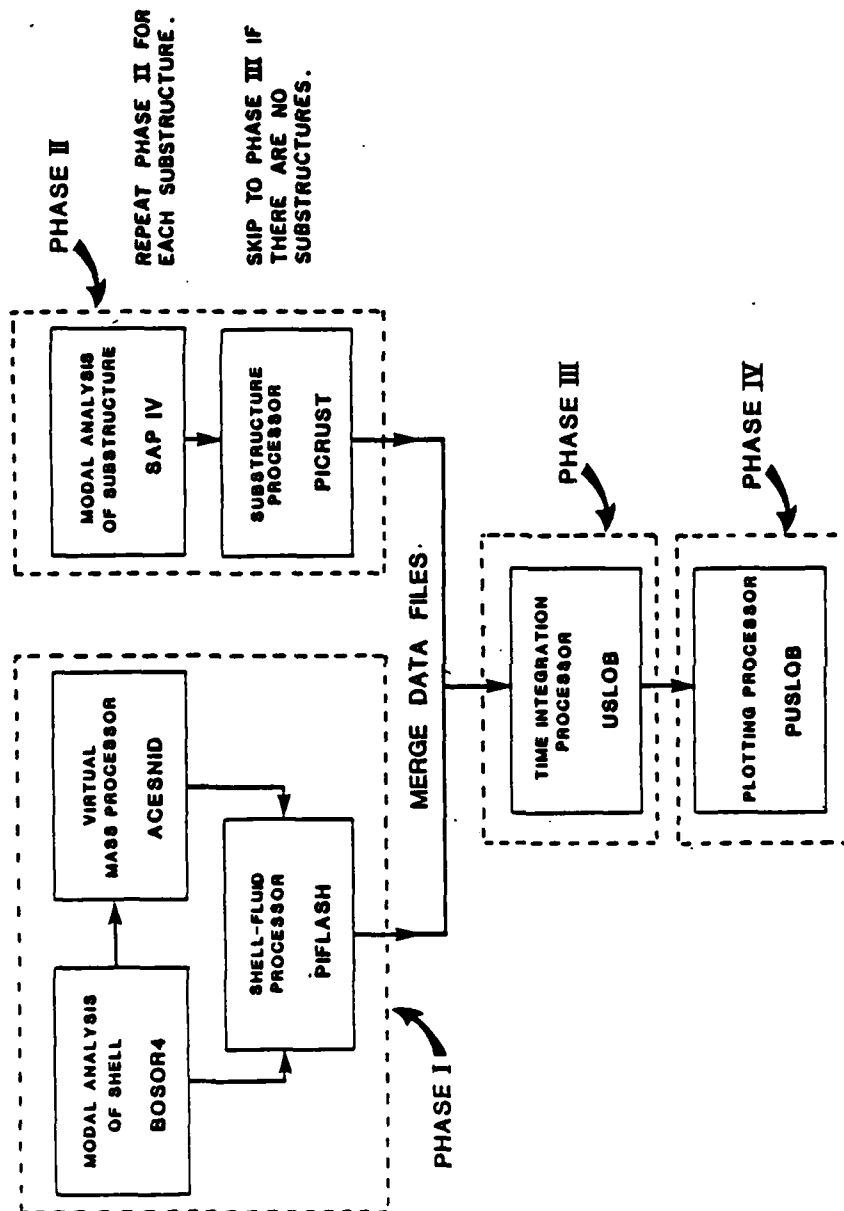


Figure 1. Organization of the ELSHOK Computer Code [Ref. 4]

7) PUSLOB--plotting processor

Figure 1 illustrates the general relationship between the programs which make up the ELSHOK computer code. As can be seen, the operation is divided into four phases.

1. Phase I--Shell and Fluid Analysis

The first step of the ELSHOK calculation is to determine the in-vacuo free-free modes and natural frequencies of the shell. This is accomplished by modeling the shell using the BOSOR4 finite difference code. This code applies to segmented, ring-stiffened, branched shells of revolution having various meridional geometries, wall constructions, and ring reinforcements making it well suited for the modeling of submarines or SSTV's. For compatibility with ELSHOK, a separate BOSOR4 calculation must be performed for each circumferential harmonic (N) included in the analysis. Examples of different harmonics in the circumferential distributions include $N = 0$ (breathing/torsional) and $N = 1$ (pure translation/whipping) as shown in Figure 2.

The second part of Phase I is the computation of the virtual mass array using ACESNID. This provides the late-time contribution of the DAA. The virtual mass array is determined from the solution, based on simple sources of a low-frequency steady-state problem in which normal displacements corresponding to surface expansion functions are applied to the surface of revolution in the infinite

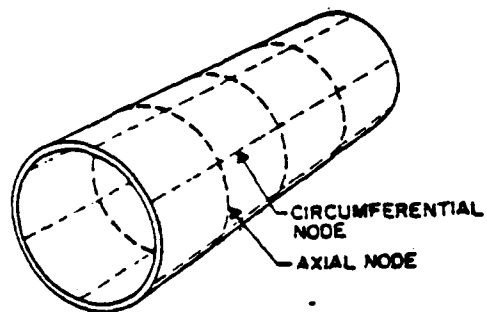
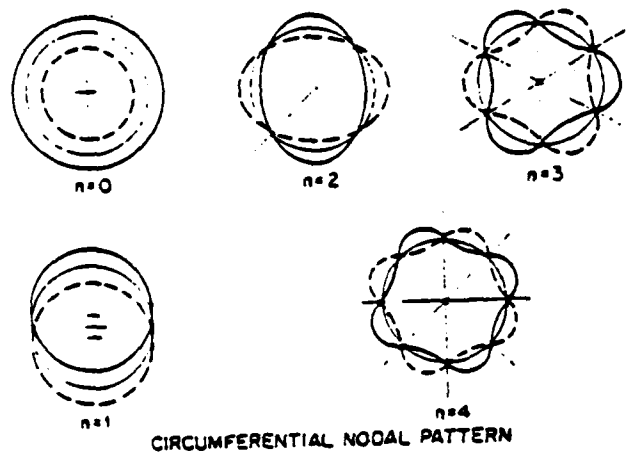


Figure 2. Nodal Patterns for Cylindrical Shells

fluid having the same shape and size as the net surface of the shell. ACESNID requires only one execution for all values of N considered.

The execution of PIFLASH completes Phase I by combining the outputs from BOSOR4 and ACESNID to create a "shell-fluid file" which contains all the information required to describe the shell during subsequent operations. One of the useful features of ELSHOK is the fact that any number of substructures can be analyzed for a given shell without having to repeat Phase I calculations.

2. Phase II--Substructure Analysis

The analysis of the substructure is performed using the SAPIV finite element code. The SAPIV code contains a variety of finite elements (plates, beams, pipes, etc.) which can be used in the modeling process. It is a general purpose code based upon a lumped mass formulation applying to linearly elastic structures. The PICRUST code takes data from SAPIV and reorganizes it to facilitate the solution of the equations governing the transient response problem under study. It is during the execution of PICRUST that the connectivity between the substructure and the shell is accounted for and influence coefficients for evaluating the forces developed at the points of attachment are calculated.

3. Phase III--Submerged Shock Response

In order to prepare a combined shell-substructure input for the USLOB time integration processor, the

shell-fluid file from Phase I is merged with the substructure files from Phase II. USLOB is the portion of the ELSHOK code which contains the underwater shock from an arbitrary point. It allows pressure-time history inputs for taper charge modeling or an exponentially decaying pressure impulse such as those encountered with conventional charges. It is of the form [Ref. 9]:

$$P(t) = K_1 (w^{1/3}/R)^{K_2} \exp(-t/\theta_0) \quad (1)$$

where:

$P(t)$ = incident pressure on the shell (psi)

K_1 = multiplicative constant for incident pressure

K_2 = spatial decay constant for incident pressure

t = time after arrival of shock wave at point of interest (msec)

w = weight of spherical charge (lb.)

$\theta_0 = K_3 w^{1/3} (w^{1/3}/R)^{K_4}$ = time constant of exponential decay (msec)

K_3 = multiplicative constant for time constant

K_4 = spatial decay constant for time constant

R = distance from the explosive to the point of interest (ft)

K_1 , K_2 , K_3 , and K_4 are constants which depend on explosive type. USLOB employs a modified version of the Runge-Kutta integration method to produce velocity-time histories in tabular form at user specified points on the shell and the substructure.

4. Phase IV--Plots of Velocity-Time Histories

After the velocity-time histories have been obtained, PUSLOB is utilized to display the velocity responses in a plotted format on a TEKTRONIX graphics terminal. These plots are adequate for viewing trends and general responses, however for formal display purposes, the IBM Versatec plotter yields a superior product. Appendix A contains a code which was written to convert the velocity punch-card files created by PUSLOB into a data format which is acceptable for Versatic plotting using the EASYPLOT program.

III. MODEL USED IN THE ANALYSIS

A. SHELL MODEL

The shell used in this analysis is a small-scale model of a typical SSTV used for conducting underwater shock tests on high-impact shipboard machinery. As can be seen in Figure 3, it is a high strength steel free-free ring stiffened cylinder with aluminum endplates. Appendix B includes a sample BOSOR4 input for one of the circumferential harmonic distributions. Data can be input to BOSOR4 using a formatted input code or by responding interactively to a set of prompts. Each segment is modeled separately which allows for different materials and physical properties to be included in the structure. The small stiffeners along the shell are represented by an orthotropic approximation which in effect increases the density of the shell. The six discrete rings are modeled individually, allowing for different size or material. The torsional rigidity (GJ) for each ring is found using the following relation:

$$GJ = EJ/2(1 + \nu) \quad (2)$$

where:

E = modulus of elasticity (psi)

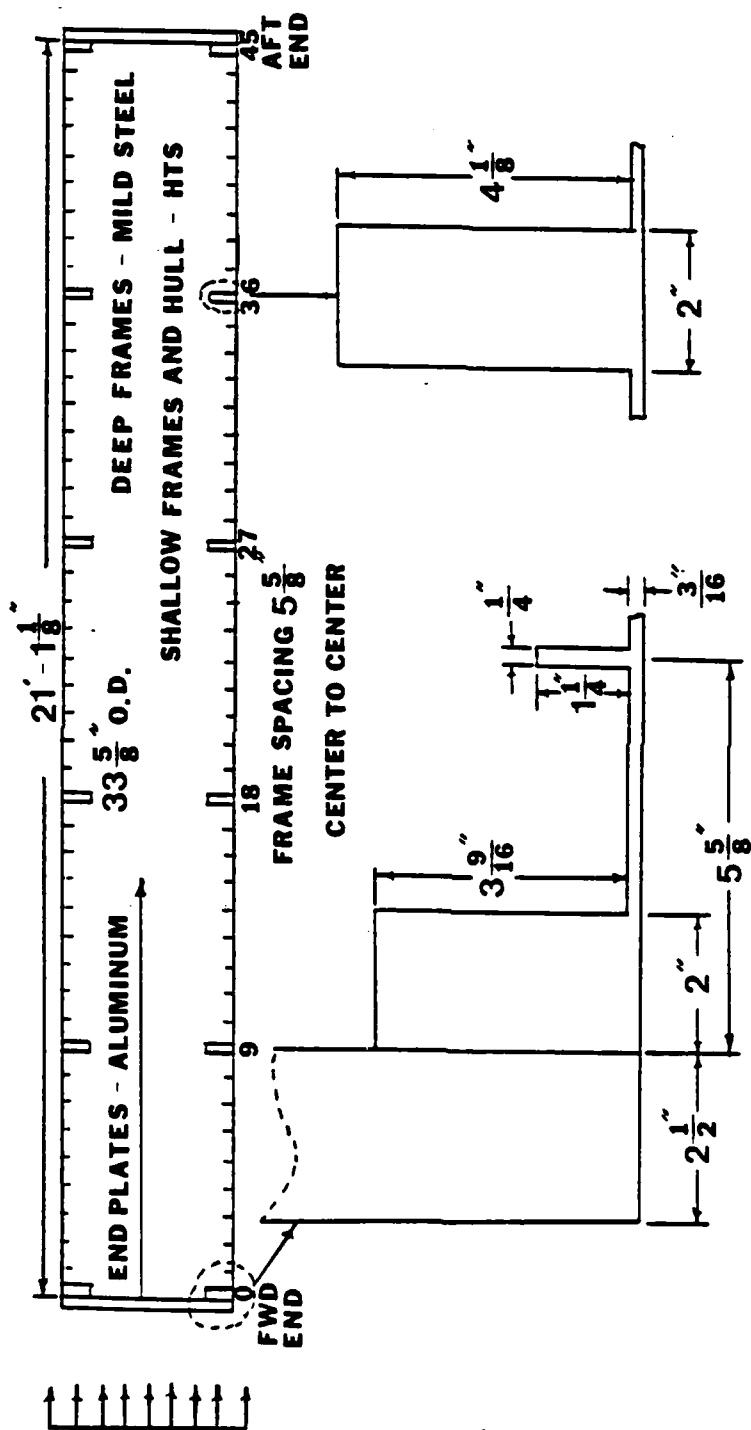


Figure 3. Ring Stiffened Cylindrical Shell Used in Analysis

$J = A^4 / (40 I_p) = \text{torsional rigidity constant [Ref. 10]}$

$\nu = \text{Poisson's ratio}$

Since the shell is a surface of revolution, the properties of each ring cross-section need only be specified at one point. The end plates (segments one and three) are divided into ten equally spaced nodes, and the cylindrical portion of the shell (segment two) is divided into forty-five nodes along the longitudinal axis. As with any finite difference code, greater accuracy will be obtained in the solution with higher numbers of nodes, however, computational time will increase. Two additional nodes are automatically inserted by BOSOR4 into each segment in order to reduce the truncation errors associated with segment interfaces and to prevent spurious vibration or buckling modes. Through finite difference techniques, BOSOR4 determines the in-vacuo free-free modes and natural frequencies of the shell. Since this study deals strictly with end-on loading, the problem is axisymmetric about the longitudinal axis. Although only the $N = 0$ (breathing/torsional) modes are activated, a few $N = 1$ (translational) models must be calculated and retained due to the fact that the ELSHOK computer code was developed for side-on loading and, therefore, requires a translational input. Since there is no translation, the solution is not affected by these superfluous modes. BOSOR4 generates a shell file which

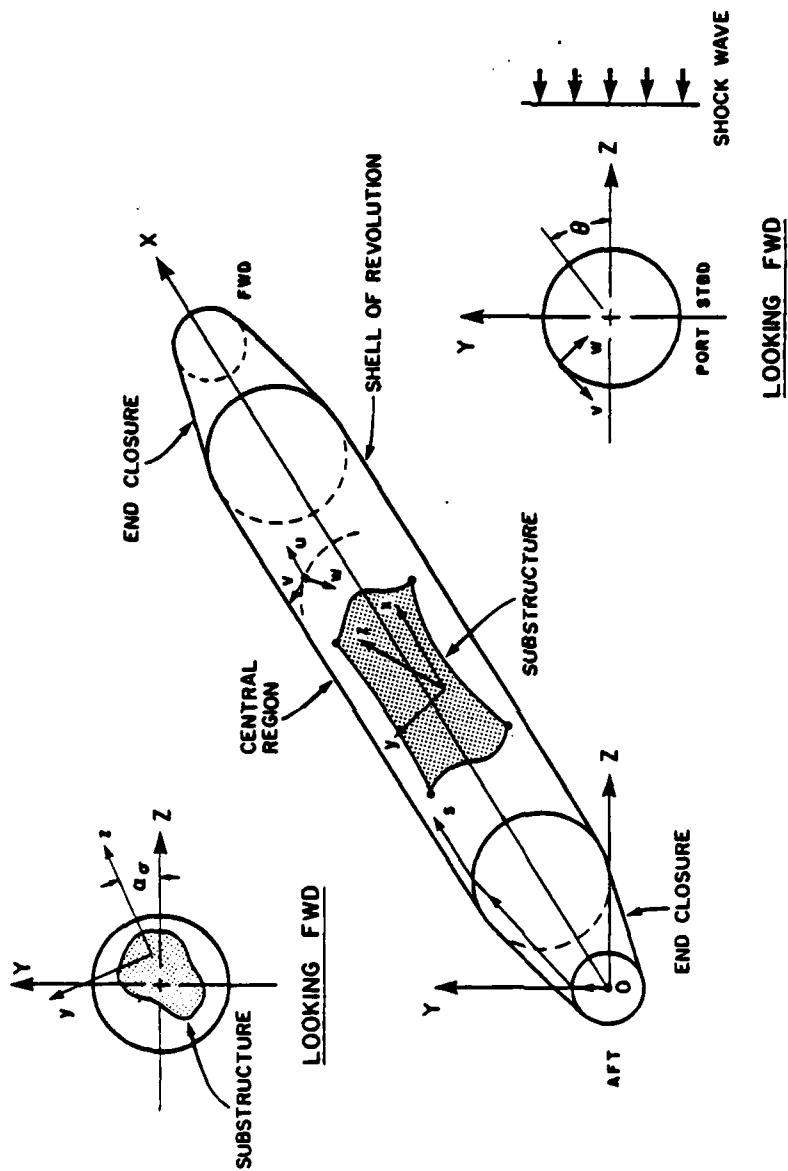


Figure 4. Typical Shell-Substructure Configuration [Ref. 4]

gives the mode shapes for each natural frequency. All breathing modes have been retained for further study, however, the torsional modes have been dropped from the analysis since they are not activated by an end-on load. Table I contains a listing of modes and natural frequencies retained for input into the PIFLASH program.

Figure 4 gives a representation of a typical shell-substructure configuration. The two coordinate systems used in an ELSHOK analysis are illustrated. X, Y, and Z refer to the global coordinate system of the shell, while x, y, and z refer to the local coordinate system of the substructure. In both systems, the x-axes run longitudinally down the hull. The substructure z-axis is related to the global Z-axis by an angle α_σ where σ refers to the substructure. Points on the wet surface of the shell are located by specifying the meridional arc length s, measured along the reference surface, and the circumferential coordinate angle θ . The lower case u, v, and w are used for local shell displacements. To eliminate torsional modes from consideration, all N = 0 modes in the shell file with significant v-displacements are discarded.

Once the shell files have been obtained from BOSOR4, the input code for ACESNID can be created. This program determines the virtual mass array which produces the late-time contribution of the DAA. It considers a cavity in an

TABLE I
MODES AND NATURAL FREQUENCIES OF SHELL

MODE	N	FREQUENCY (HZ)
2	0	1.259E-03
4	0	2.239E+02
6	0	3.850E+02
7	0	4.761E+02
9	0	5.935E+02
12	0	7.826E+02
13	0	9.369E+02
14	0	1.048E+03
19	0	1.584E+03
20	0	1.585E+03
21	0	1.596E+03
22	0	1.598E+03
23	0	1.656E+03
25	0	1.791E+03
26	0	1.818E+03
27	0	1.856E+03
28	0	1.878E+03
29	0	1.890E+03
30	0	1.898E+03
1	1	1.390E-04
2	1	6.321E+01

infinite acoustic fluid corresponding to the wet surface of the shell. A user specified number of surface expansion functions having the property of orthogonality over the wet surface of the shell are obtained during the calculation of the virtual or entrained mass. The cavity is divided into bands which describe the behavior of the fluid. A sufficient number of bands must be provided to enable the fluid response to match the normal motion specified by the surface expansion functions. In a sense, they can be looked upon as nodes in a finite element model. In this analysis, the shell is assumed to be totally immersed in salt water with a mass density of $9.59684\text{E-}05 \text{ lbf-s}^2/\text{in}^4$. The endplates are divided into fifteen bands each, and the cylinder has fifty-one bands. Six surface expansion functions have been generated for the endplates with ten along the cylinder.

The shell mode files from BOSOR4 and the virtual mass file from ACESNID are combined in the PIFLASH program to produce a shell-fluid file for further processing. The model of the shell is now complete and can be used for any variety of substructures without any recalculation.

B. SUBSTRUCTURE MODEL

The idealized internal equipment selected for study in this analysis is a high strength steel diaphragm or plate located at the discrete ring at frame nine. The SAPIV

finite element code is utilized to model the diaphragm. The diaphragm has been divided into eight "pie-shaped" wedges which are further subdivided into three sections. Twenty-four plate elements are used in this model with twenty-five nodal points. Since this study is concerned with end-on loading, the node at the center of the plate is constrained to move only in the x-direction with no rotations. The outer nodes (eighteen through twenty-five) are rigidly attached to the shell. This is accomplished through a modification of the general purpose SAPIV code by the developers of ELSHOK. During the parametric study, the diaphragm thickness is uniformly varied from .25 inches to 9.25 inches. Figure 5 is a TEKTRONIX representation of the finite element model of the substructure. Appendix B includes one of the SAPIV input codes used during the parametric study.

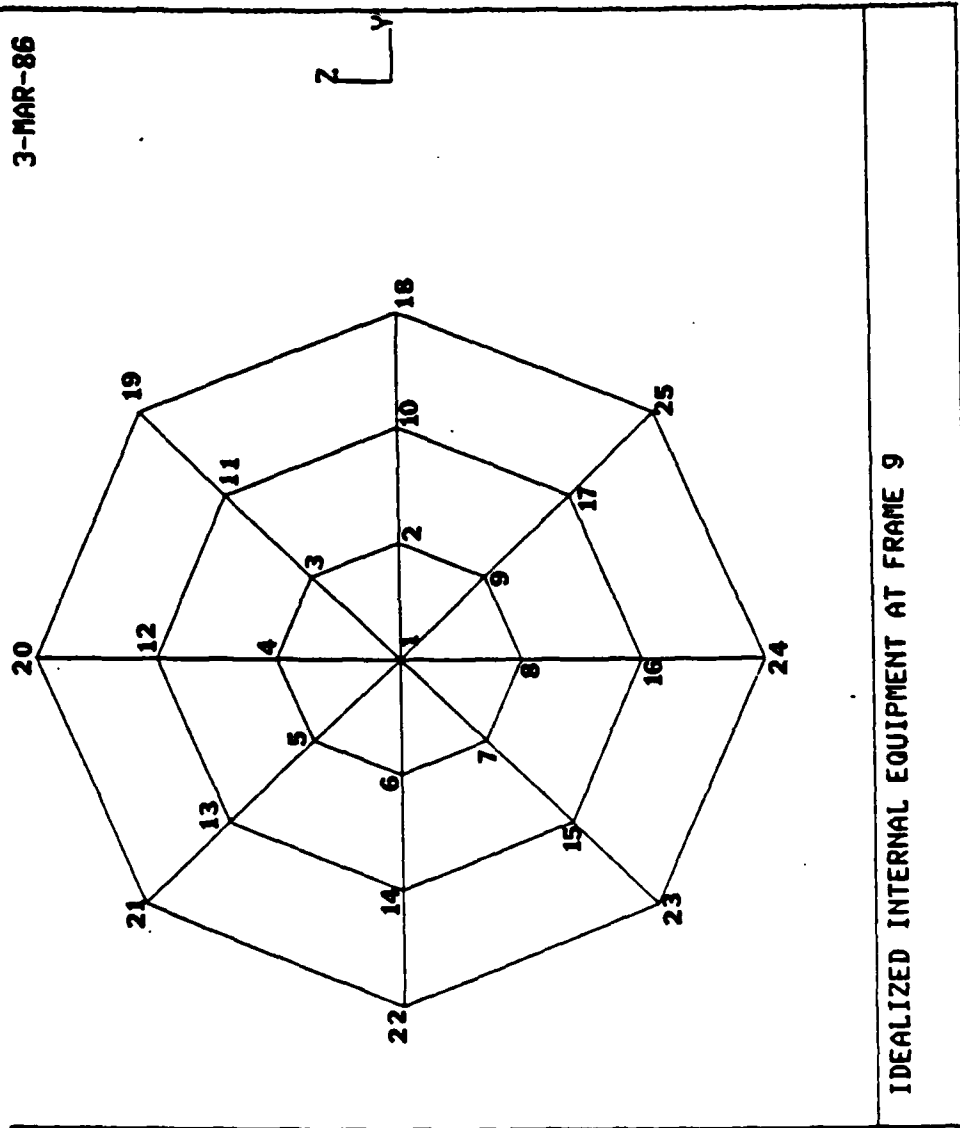


Figure 5. Finite Element Model of Diaphragm

IV. ANALYSIS

The purpose of this analysis is to study the shell/substructure interaction after the system is subjected to an end-on load while varying the mass and stiffness of the internal substructure. Two different types of loading are explored: a taper charge and a conventional charge. Taper charges are characterized by sustained incident pressure on a body over a period of time. They are used in underwater shock tests to simulate the type of pressure profile which a body would experience from a nuclear detonation. Extensive use of scaling is involved in efforts to reproduce the physical behavior of an object in response to a nuclear charge without generating the extremely high pressures associated with actual detonations. Conventional charges create a large initial pressure pulse followed by a rapidly decaying exponential. ELSHOK uses inputs of charge weight and standoff geometry to calculate the transient velocities of the shell and substructure in response to these loads.

A. ANALYSIS PROCEDURE

Once the shell model has been produced, a series of SAPIV runs are conducted for the diaphragms of increasing thickness. Each run generates natural frequencies and accompanying mode shapes for each model. The PICRUST

program reduces the data obtained through SAPIV into a format which can be combined with the shell-fluid file for processing with the USLOB code. The substructure is connected to the shell during this phase of the ELSHOK analysis. The diaphragm is attached to shell segment two at frame nine (node eleven).

The weight, type, and location of the charge is specified in the USLOB input code. To set up an end-on load referenced to the global coordinate system, the charges are placed in the negative X-direction at a distance of 70 feet (840 inches). This distance is typical of stand-off distances used during actual tests. For the taper charge, a typical incident pressure-time history shown in Figure 6 is used to simulate the shock wave loading. In order to make a meaningful comparison between the structural responses from a taper charge and a conventional charge, it is necessary that they have equivalent shock wave impulses. In the field of underwater shock analysis, "impulse" refers to the time-integral of the pressure profile [Ref. 9]. The impulse of unit area of the shock wave front up to a time t after its arrival is given by:

$$I(t) = \int_0^t P(t) dt \quad (3)$$

The impulse of the taper charge is found by calculating the area under the pressure-time history in Figure 6. As was

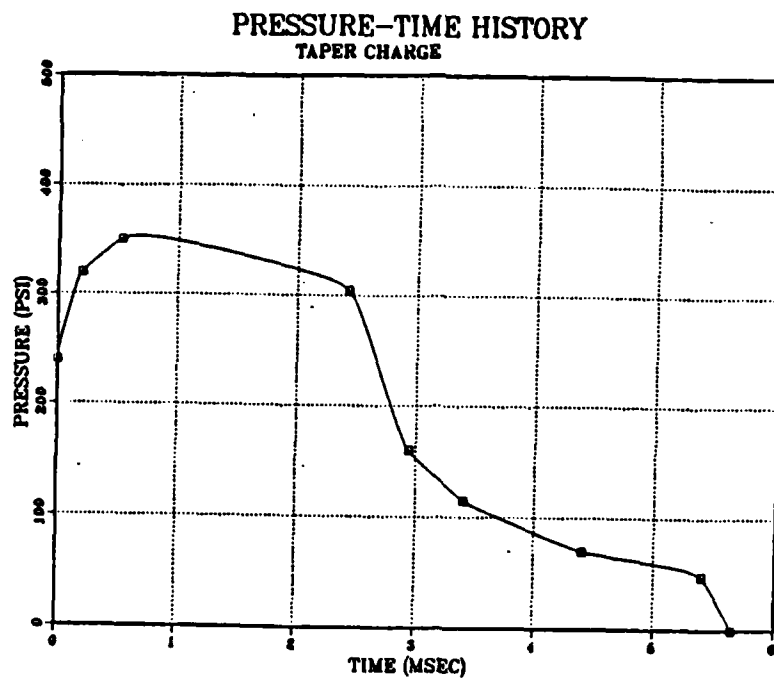


Figure 6. Incident Pressure-Time History--Taper Charge

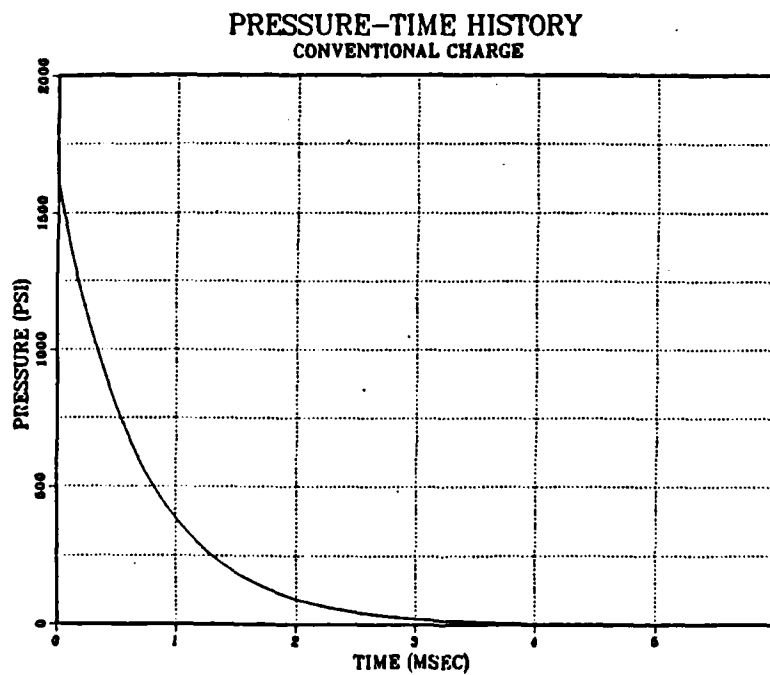


Figure 7. Incident Pressure-Time History--Conventional Charge

stated earlier, a conventional charge follows a pressure-time history given by equation (1):

$$P(t) = K_1 (w^{1/3}/R)^{K_2} \exp(-t/\theta_0) \quad (1)$$

where:

$$\theta_0 = K_3 w^{1/3} (w^{1/3}/R)^{K_4} = \text{time constant of exponential decay (msec)}$$

HBX-1 is a popular explosive used in underwater shock tests, so it was decided to use it in this study for the conventional charge. K_1 , K_2 , K_3 , and K_4 are constants which depend on the type of explosive used. The values used in this study are [Ref. 11]:

$$K_1 = 3.8354314E+05$$

$$K_2 = 1.144$$

$$K_3 = 3.03131E-05$$

$$K_4 = -.247$$

By matching the impulses between the taper charge and the conventional charge, a charge weight of 352 lbs of HBX-1 is found to yield an equivalent impulse. The peak pressure generated by the charge is 1620 psi which creates the incident pressure-time history shown in Figure 7. The conventional charge expends most of its impulse in the first

millisecond, while the taper charge takes over four milliseconds to expend an equivalent amount of impulse. Because of the sharp rise in pressure experienced from a conventional charge, a higher transient response is developed in the shell than with a taper charge of equivalent impulse.

After selecting suitable charges, the time step increment and integration limits are specified in the USLOB input code. Through a trial and error process, enough time steps are chosen to identify the significant interactions between the shell and substructure. It was found that 1600 time steps for an 80 msec time period gave an adequate illustration of the system response. The USLOB program enables the user to examine the velocity-time history response of various nodes in tabular form. This gives some indication of whether the run was successful, however, the plots from PUSLOB are required before response characteristics can be identified.

To obtain a baseline velocity-time history, a complete analysis is performed on the submerged empty stiffened shell. From the velocity-time history plots, the dominant frequency from the computed shock response is observed. Provided the mass of the diaphragm remained small with respect to the shell, it was felt that this provided a good estimation of the excitation frequency for the diaphragm. The dominant frequency is 187.80 Hz for the taper charge and

195.44 Hz for the conventional charge. A series of SAPIV calculations are conducted on diaphragms of varying thickness in order to identify the fundamental frequency of each substructure. These values are given in Table II. An analysis is performed on the shell/substructure system for each diaphragm thickness to observe the coupled velocity-time history response as the substructure mass grows in relation to that of the shell.

TABLE II
FUNDAMENTAL FREQUENCIES OF DIAPHRAGM SUBSTRUCTURE

Thickness (In)	Frequency (Hz)
.25	43.66
.50	87.31
.75	130.97
1.00	174.59
1.05	183.35
1.06	185.10
1.07	186.85
1.10	192.10
1.15	200.85
1.25	218.20
2.25	392.95
3.25	567.55
4.25	742.14
5.25	916.73
6.25	1091.33
7.25	1265.92
8.25	1440.51
9.25	1615.42

V. RESULTS

The velocity time-history response begins at time zero when the incident pressure wave from the underwater explosion strikes the shell. With end-on loading, the forward endplate receives the initial contact with velocity indicated along the longitudinal axis. The empty shell response is analyzed first, followed by a discussion of the coupled effects when the diaphragm achieves resonance.

A. VELOCITY-TIME HISTORY RESPONSE--EMPTY SHELL

The empty shell velocity-time history responses for the conventional and taper charges are contained in Figures 8 through 20. It can be seen that the conventional charge causes a much greater transient response in the shell. In both cases, the velocity is rapidly damped by interaction between the shell and the infinite fluid medium. It is interesting to observe the differences in response between the various locations on the shell. The forward endplate is perpendicular to the shock wave, receiving the full force from the incident pressure pulse. Inertial forces are generated by the endplate causing severe local deformation in the nearest nodes on the cylinder due to the rigid coupling between segments. The motion propagates down the shell along the longitudinal axis until it reaches the aft

VELOCITY RESPONSE - EMPTY SHELL SEGMENT ONE - NODE ONE

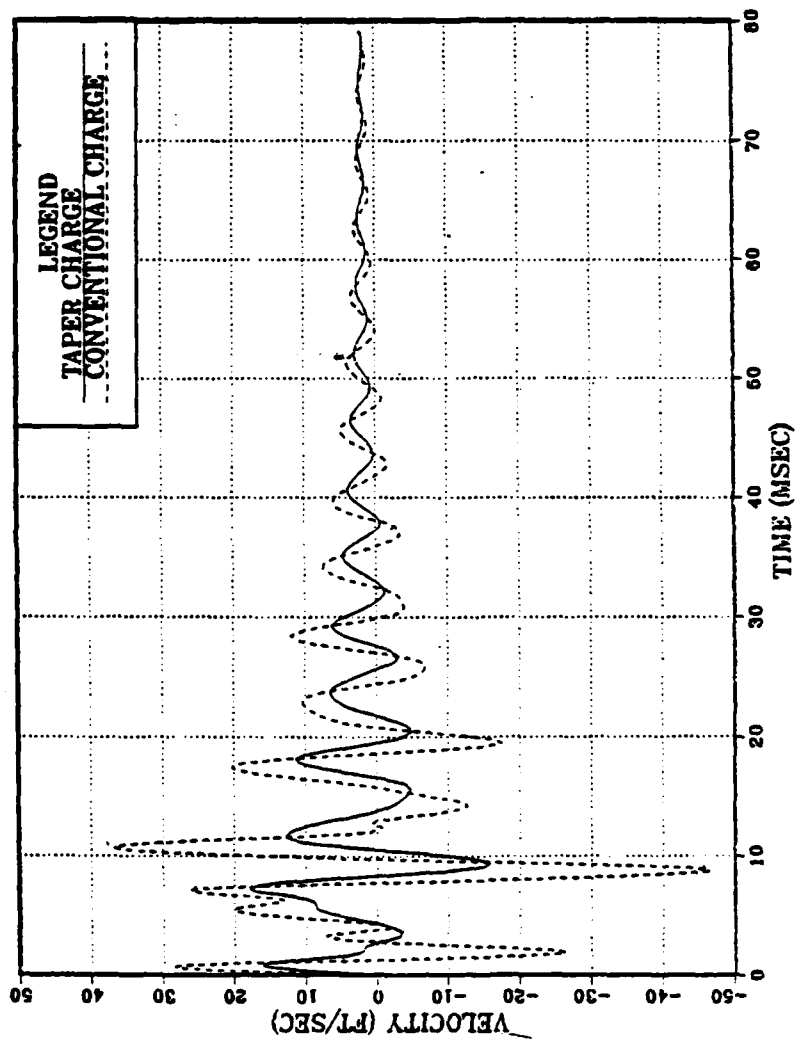


Figure 8. Velocity-Time History Response (Empty Shell) --FWD Endplate Center

VELOCITY RESPONSE - EMPTY SHELL SEGMENT TWO - NODE TWO

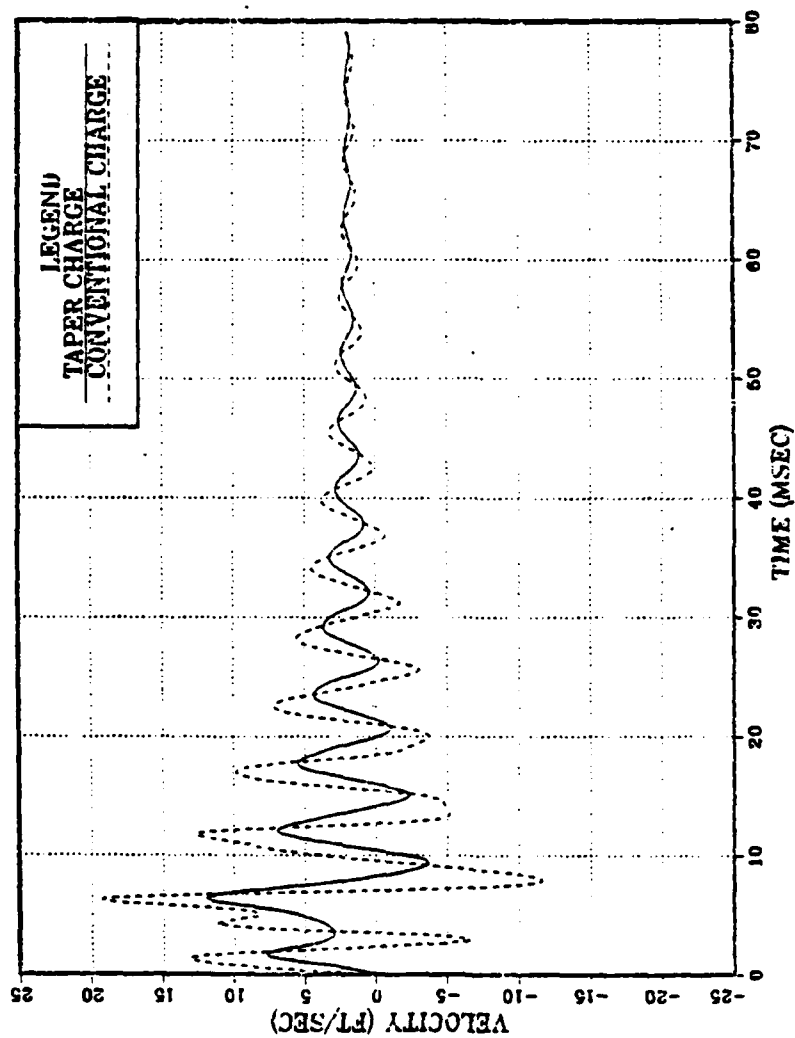


Figure 9. Velocity-Time History Response (Empty Shell) --Frame Zero

VELOCITY RESPONSE - EMPTY SHELL

SEGMENT TWO - NODE SEVEN

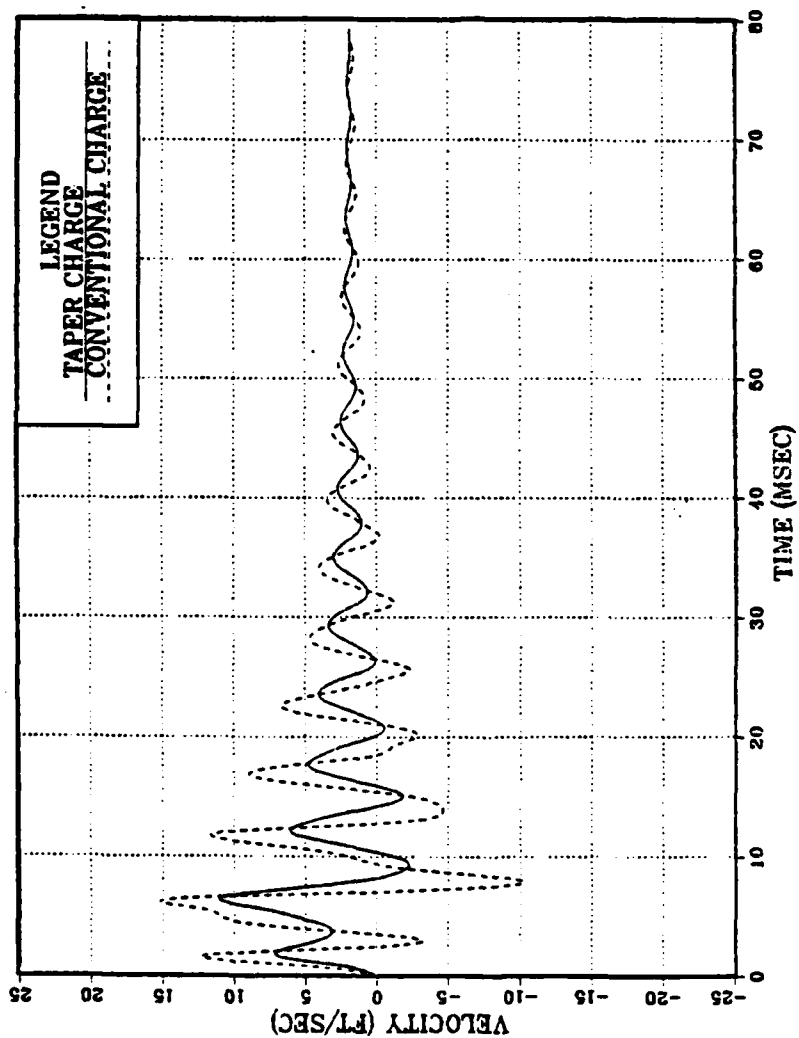


Figure 10. Velocity-Time History Response (Empty Shell) --Frame Five

VELOCITY RESPONSE - EMPTY SHELL

SEGMENT TWO - NODE ELEVEN

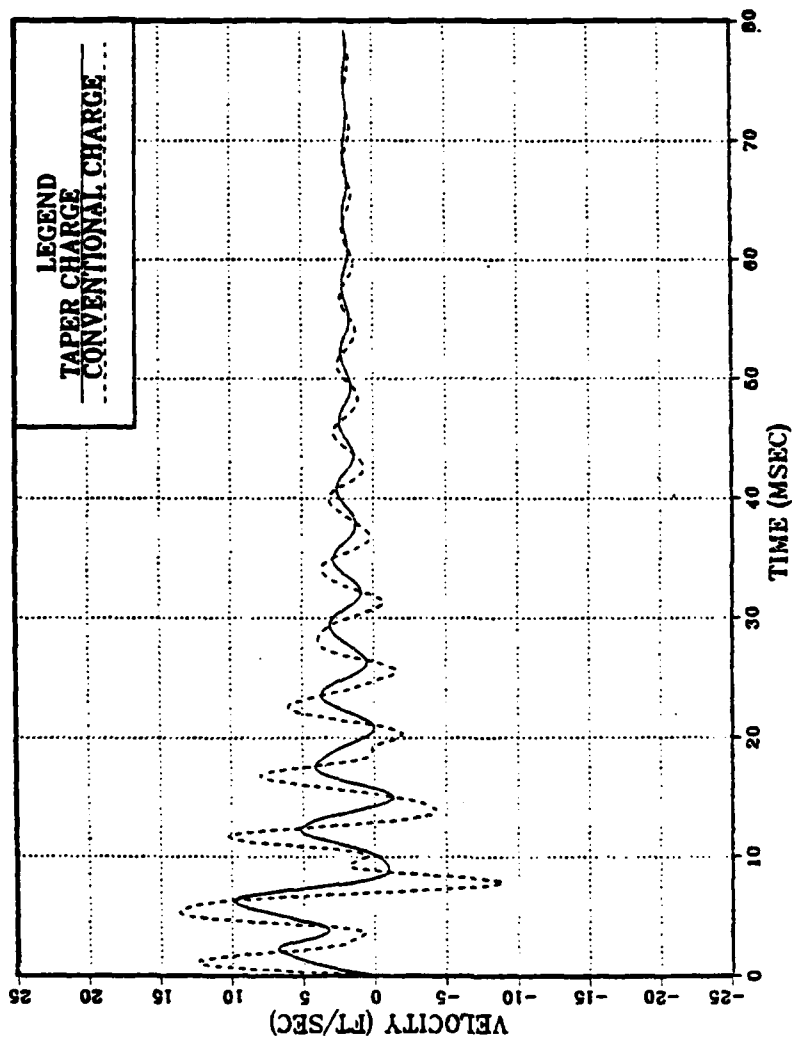


Figure 11. Velocity-Time History Response (Empty Shell) --Frame Nine

VELOCITY RESPONSE - EMPTY SHELL

SEGMENT TWO - NODE FIFTEEN

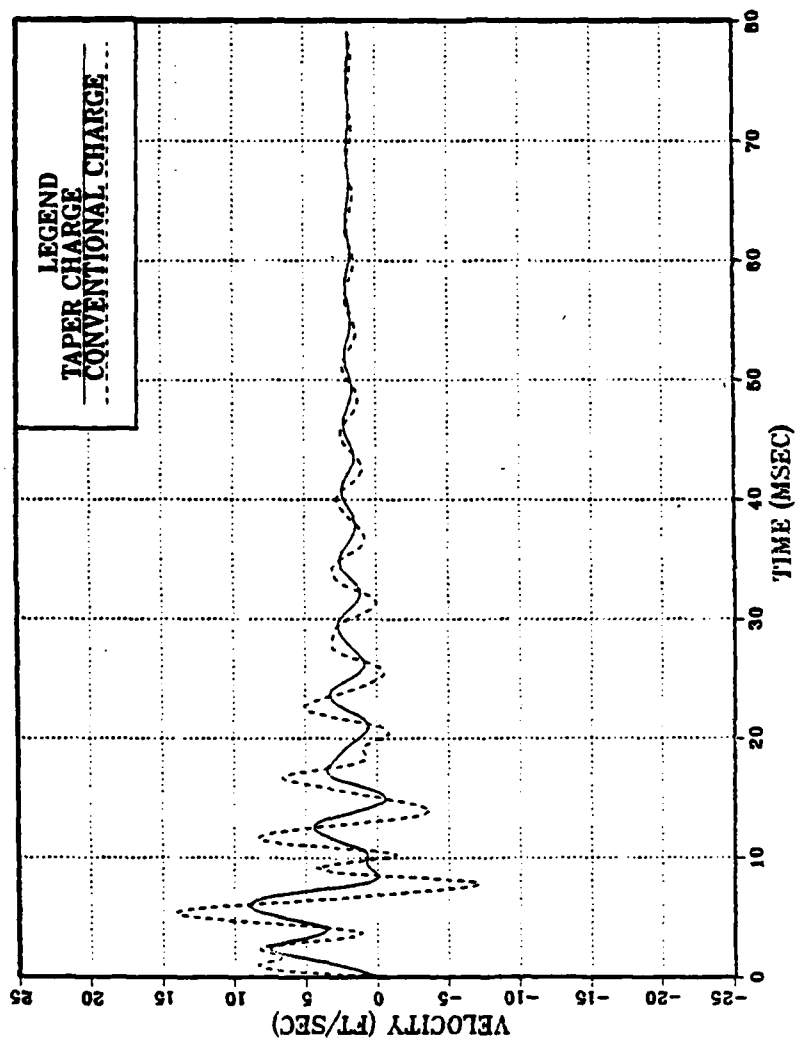


Figure 12. Velocity-Time History Response (Empty Shell) --Frame Thirteen

VELOCITY RESPONSE - EMPTY SHELL

SEGMENT TWO - NODE TWENTY

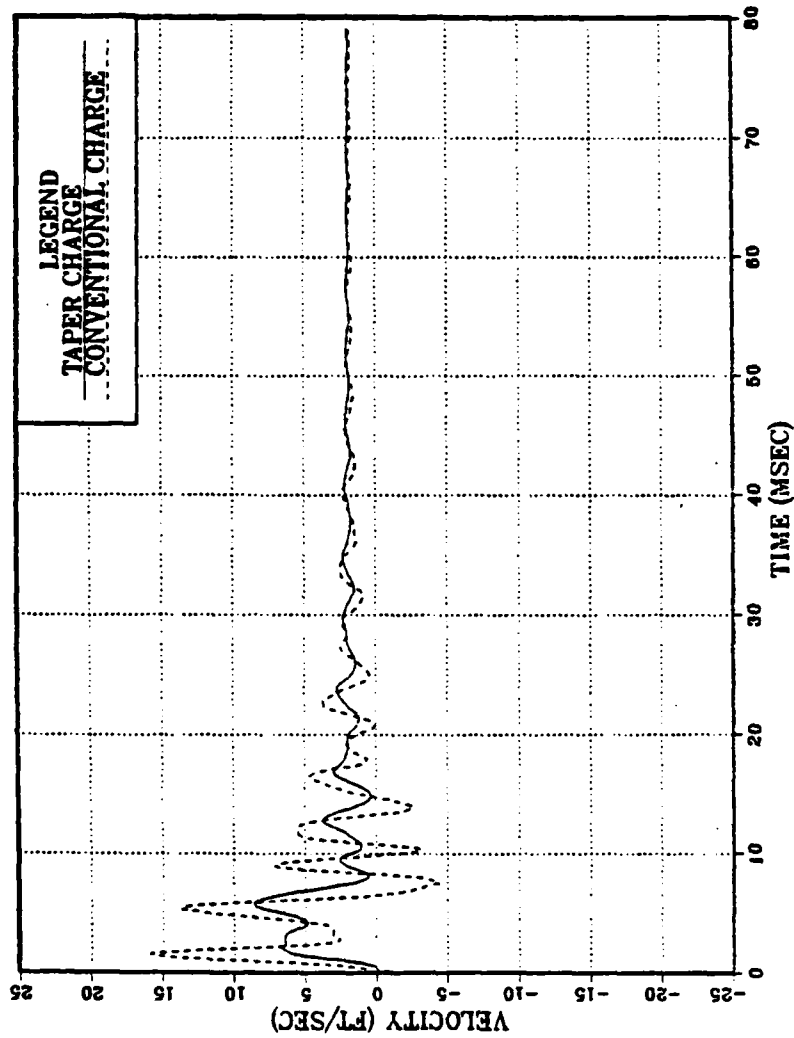


Figure 13. Velocity-Time History Response (Empty Shell)--Frame Eighteen

VELOCITY RESPONSE - EMPTY SHELL SEGMENT TWO - NODE TWENTY FOUR

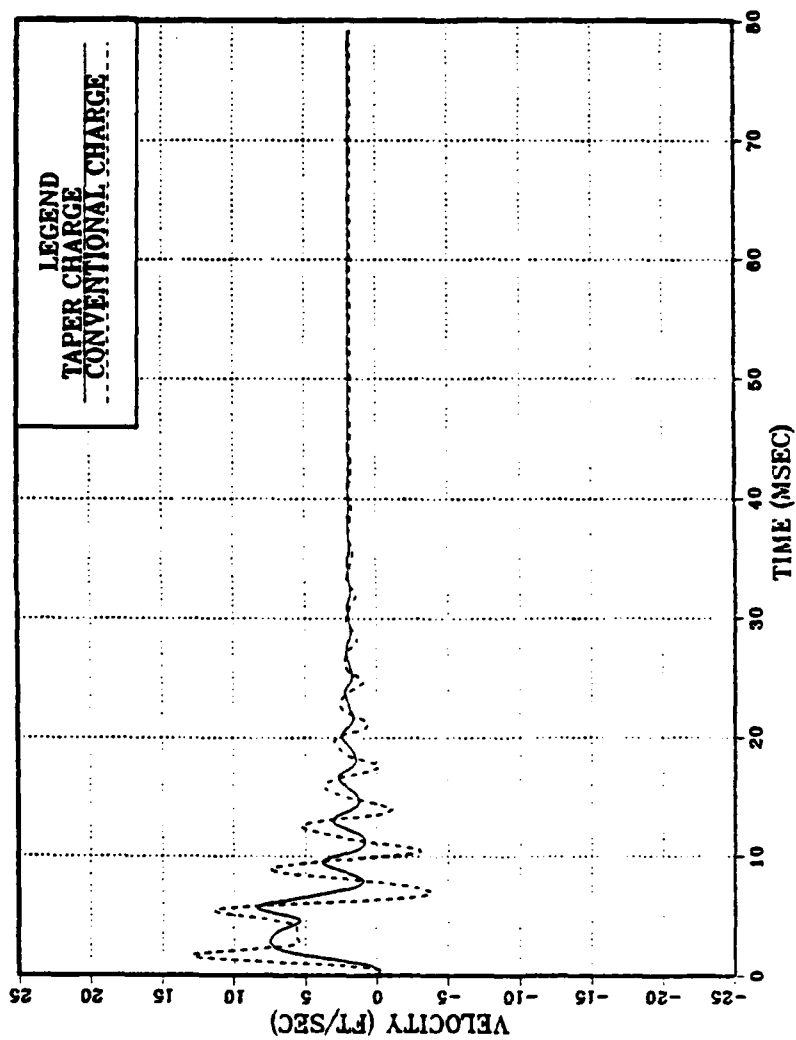


Figure 14. Velocity-Time History Response (Empty Shell) --Frame Twenty-Three

VELOCITY RESPONSE - EMPTY SHELL SEGMENT TWO - TWENTY EIGHT

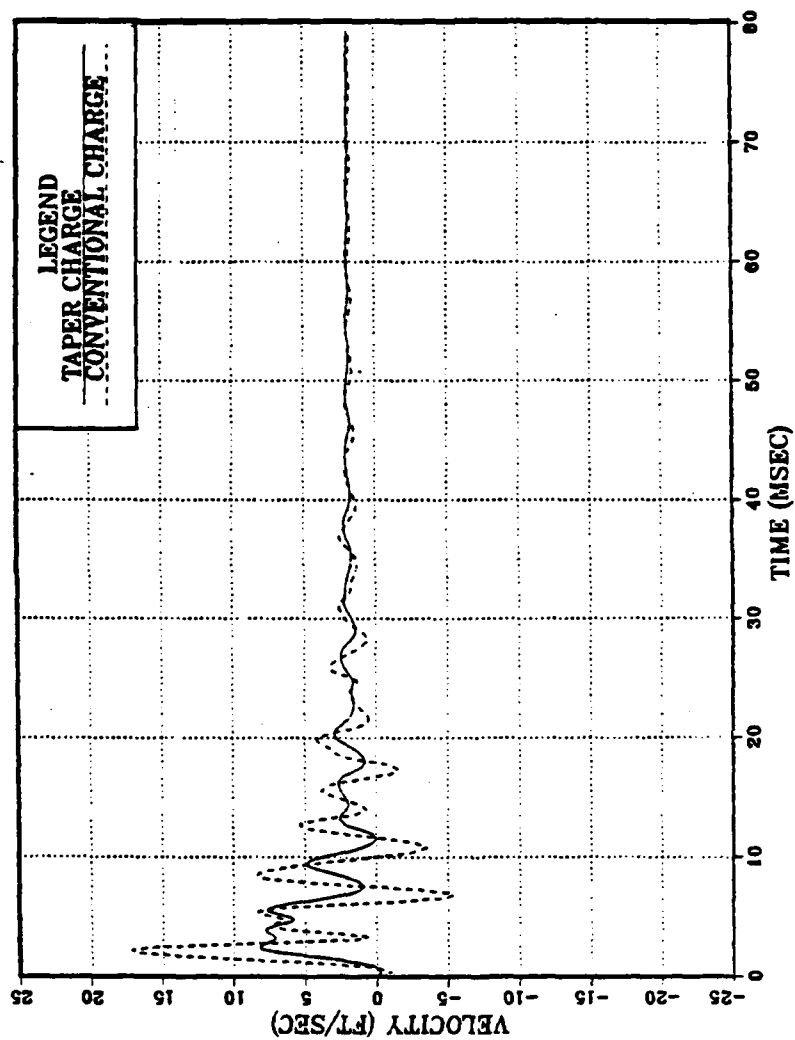


Figure 15. Velocity-Time History Response (Empty Shell) --Frame Twenty-Seven

VELOCITY RESPONSE - EMPTY SHELL SEGMENT TWO - NODE THIRTY THREE

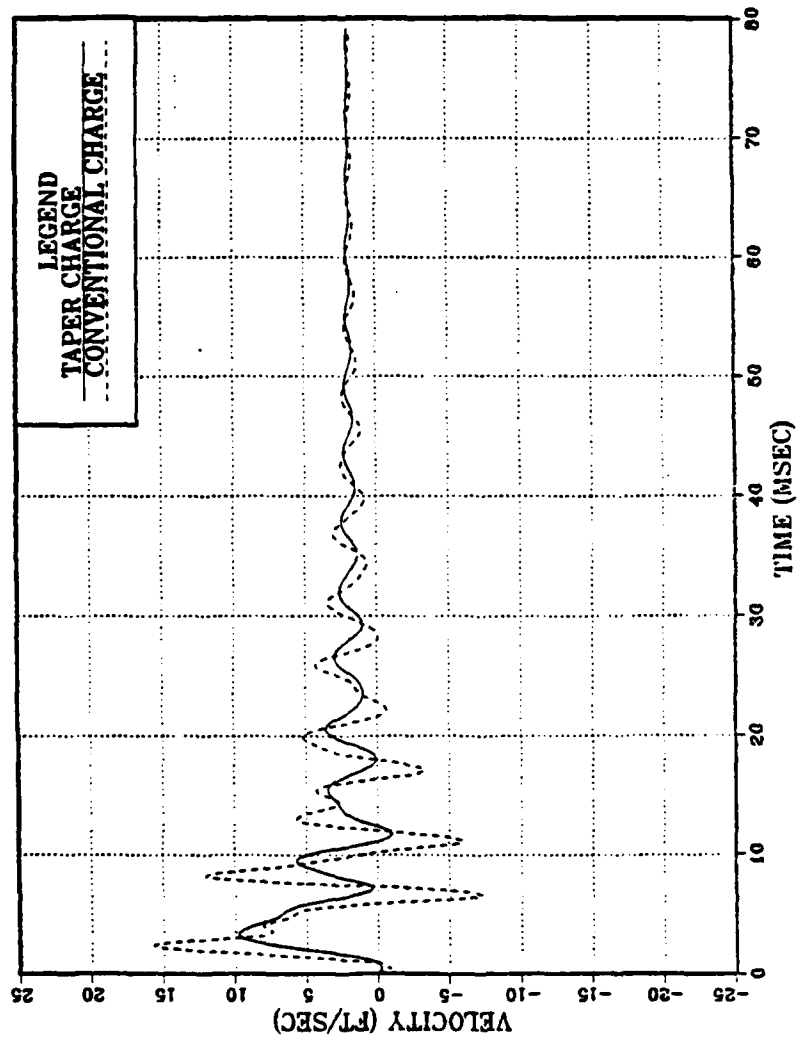


Figure 16. Velocity-Time History Response (Empty Shell) ---Frame Thirty-Two

VELOCITY RESPONSE - EMPTY SHELL

SEGMENT TWO - NODE THIRTY SEVEN

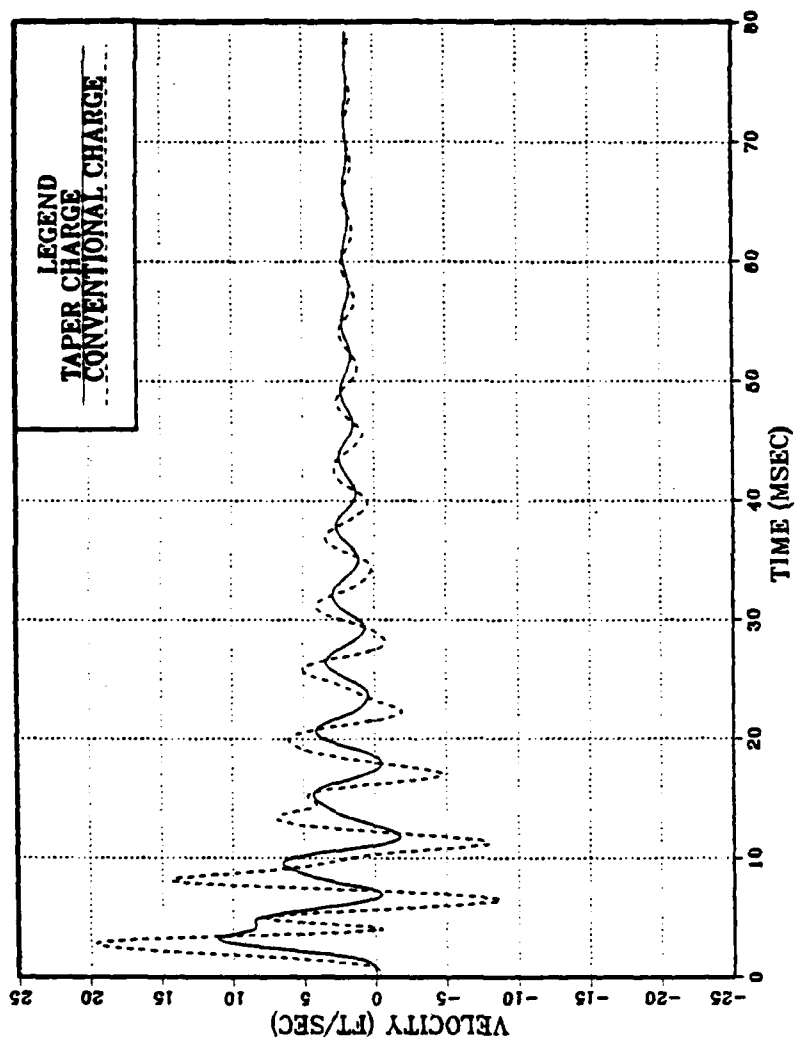


Figure 17. Velocity-Time History Response (Empty Shell) --Frame Thirty-Six

VELOCITY RESPONSE - EMPTY SHELL SEGMENT TWO - NODE FORTY ONE

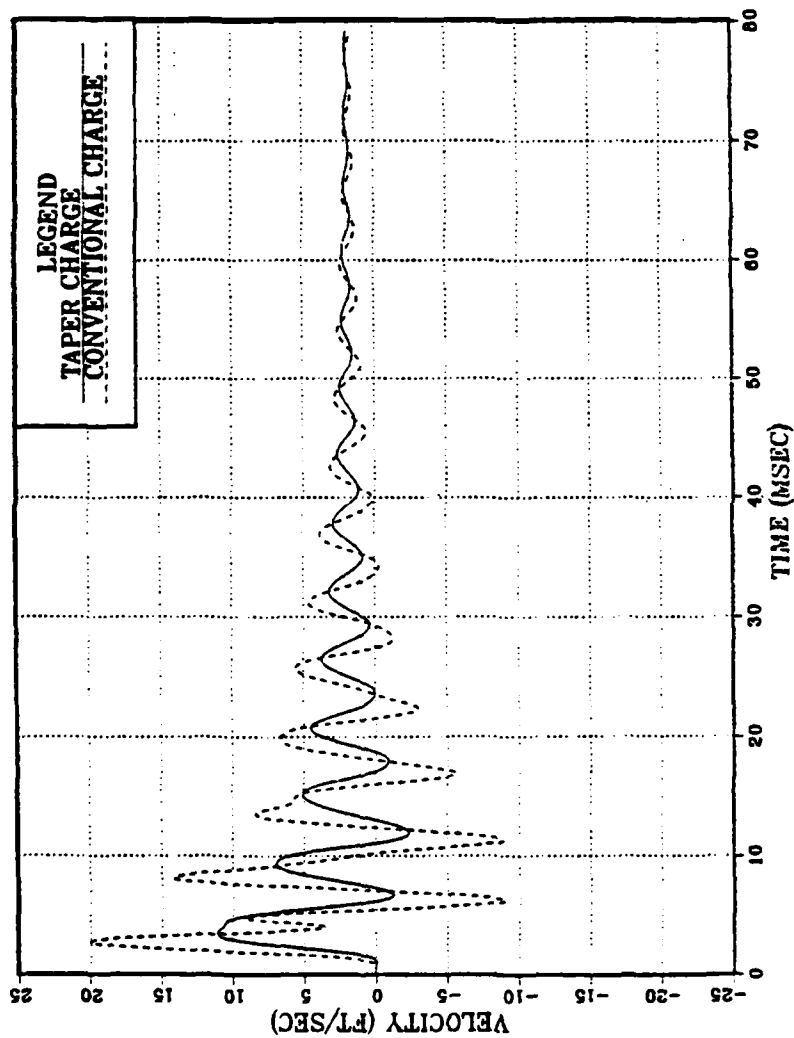


Figure 18. Velocity-Time History Response (Empty Shell) --Frame Forty

VELOCITY RESPONSE - EMPTY SHELL SEGMENT TWO - NODE FORTY SIX

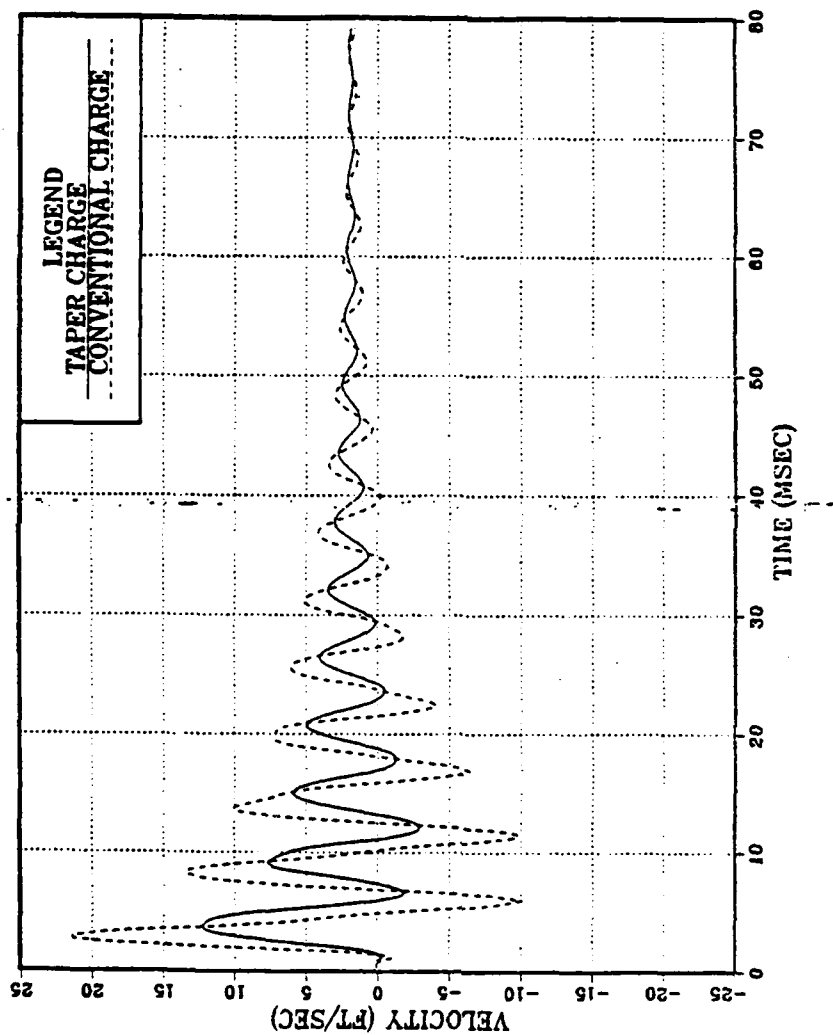


Figure 19. Velocity-Time History Response (Empty Shell) --Frame Forty-Five

VELOCITY RESPONSE - EMPTY SHELL SEGMENT THREE - NODE TWELVE

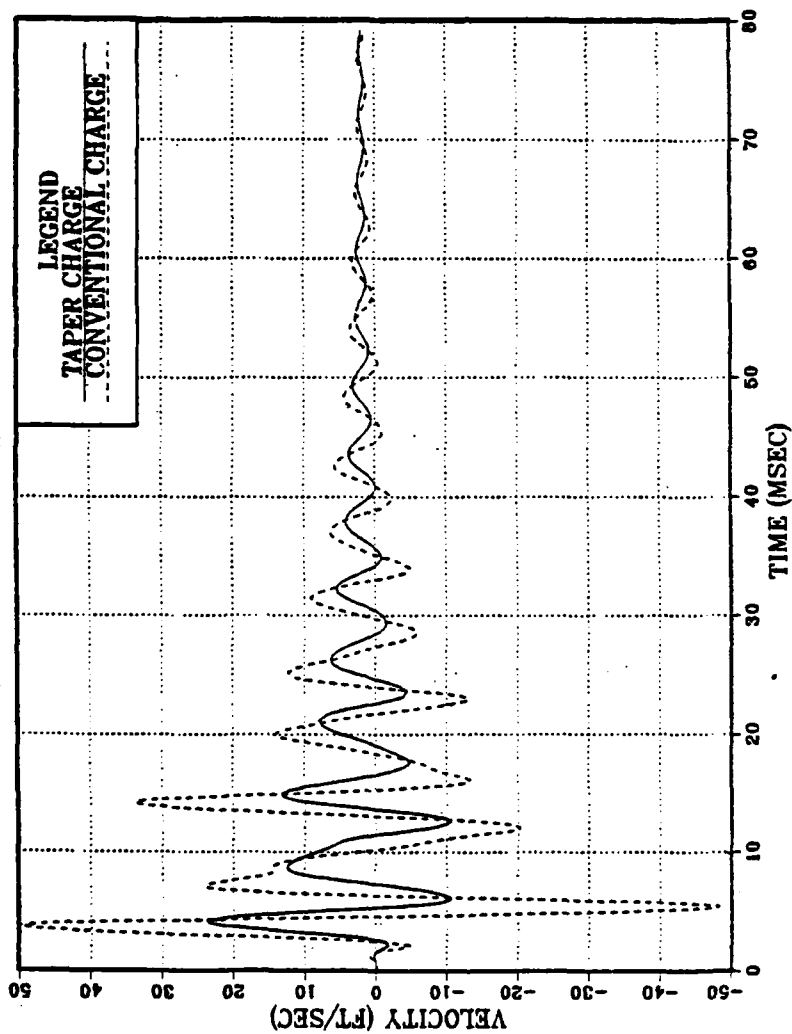


Figure 20. Velocity-Time History Response (Empty Shell) --AFT Endplate Center

endplate over a millisecond after initial shock wave contact. At first the aft endplate moves in the negative X-direction as the "ripple" proceeds down the structure. Then it experiences a violent transient response as it is affected not only by the inertial forces from the shell, but by the reflected pressure pulses from the water it displaces. After the initial shock, the shell settles into an "accordion" effect, expanding and contracting as the forward and aft endplates move in opposite directions.

B. VELOCITY-TIME HISTORY RESPONSE--COUPLED SHELL/ SUBSTRUCTURE SYSTEM

From the results of the analyses performed on the coupled shell/substructure system, Tables III and IV were created in order to identify when the diaphragm achieved resonance. $\Omega/\bar{\Omega}$ is the frequency ratio between the fundamental frequency of the simply-supported diaphragm (Ω) and the dominant frequency observed in the velocity-time history response of the submerged empty stiffened shell ($\bar{\Omega}$). M_1/M_2 is the mass ratio between the substructure (M_1) and the shell with endplates (M_2). Figure 21 is a plot of the velocity of the diaphragm center versus the frequency ratio $\Omega/\bar{\Omega}$. It reveals that in both the taper and conventional charge responses, the diaphragm achieves its maximum velocity or resonance when the fundamental frequency of the substructure is nearly equal to the excitation frequency from the shell. Resonance occurs when the mass ratio is approximately .08. Since

TABLE III

MAXIMUM VELOCITY RESPONSE OF DIAPHRAGM SUBSTRUCTURE
WITH VARYING THICKNESS (TAPER CHARGE)

Thickness (In)	$\Omega/\bar{\Omega}$	M1/M2	Velocity (ft/sec)
.25	.232	.018	22.19
.50	.465	.036	16.64
.75	.762	.055	20.79
1.00	.930	.073	34.81
1.05	.976	.076	35.65
1.06	.986	.077	35.78
1.07	.995	.078	35.65
1.10	1.023	.080	33.58
1.15	1.069	.084	30.36
1.25	1.162	.091	26.24
2.25	2.092	.164	11.61
3.25	3.022	.237	10.60
4.25	3.952	.310	9.04
5.25	4.881	.383	8.70
6.25	5.811	.456	8.44
7.25	6.741	.528	8.15
8.25	7.670	.601	7.87
9.25	8.602	.674	7.62

TABLE IV

MAXIMUM VELOCITY RESPONSE OF DIAPHRAGM SUBSTRUCTURE
WITH VARYING THICKNESS (CONVENTIONAL CHARGE)

Thickness (In)	$\alpha/\bar{\alpha}$	M1/M2	Velocity (ft/sec)
.25	.223	.018	40.42
.50	.447	.036	28.26
.75	.670	.055	45.29
1.00	.893	.073	68.73
1.05	.938	.076	73.84
1.06	.947	.077	74.71
1.07	.956	.078	74.22
1.10	.983	.080	69.69
1.15	1.028	.084	62.90
1.25	1.116	.091	62.75
2.25	2.011	.164	21.77
3.25	2.904	.237	17.67
4.25	3.797	.310	15.51
5.25	4.691	.383	13.69
6.25	5.584	.456	12.01
7.25	6.477	.528	11.37
8.25	7.371	.601	11.00
9.25	8.265	.674	10.69

DIAPH MAX VEL VS NORMALIZED FREQ

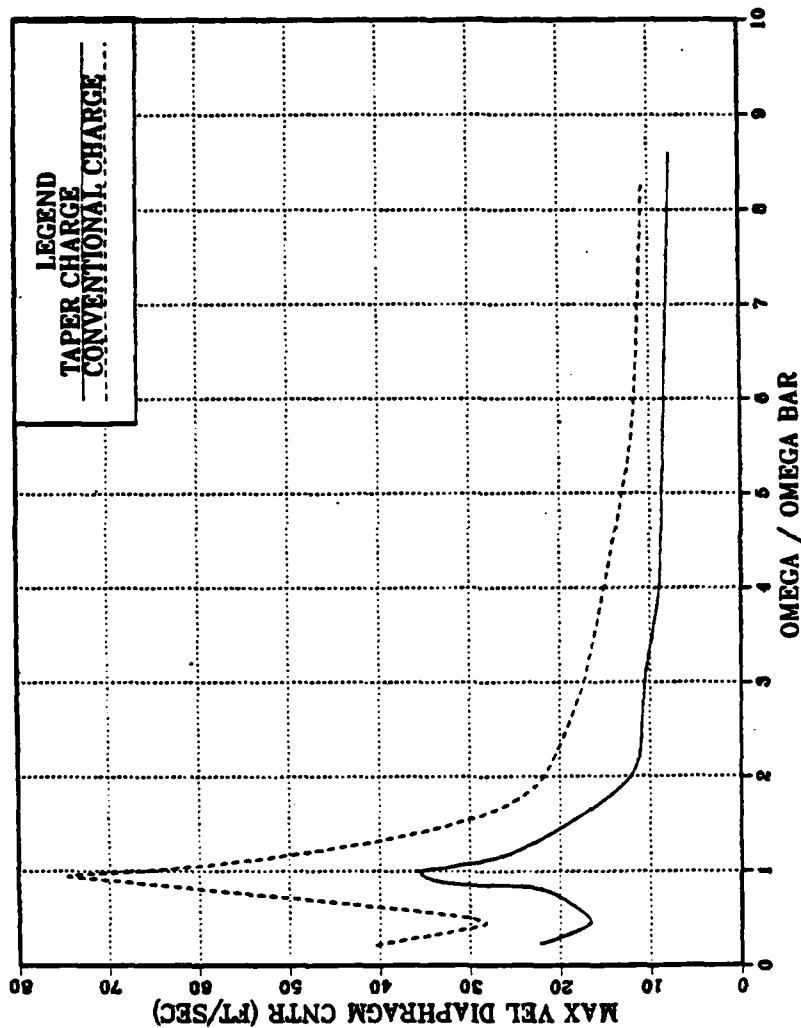


Figure 21. Diaphragm Maximum Velocity vs. Normalized Frequency

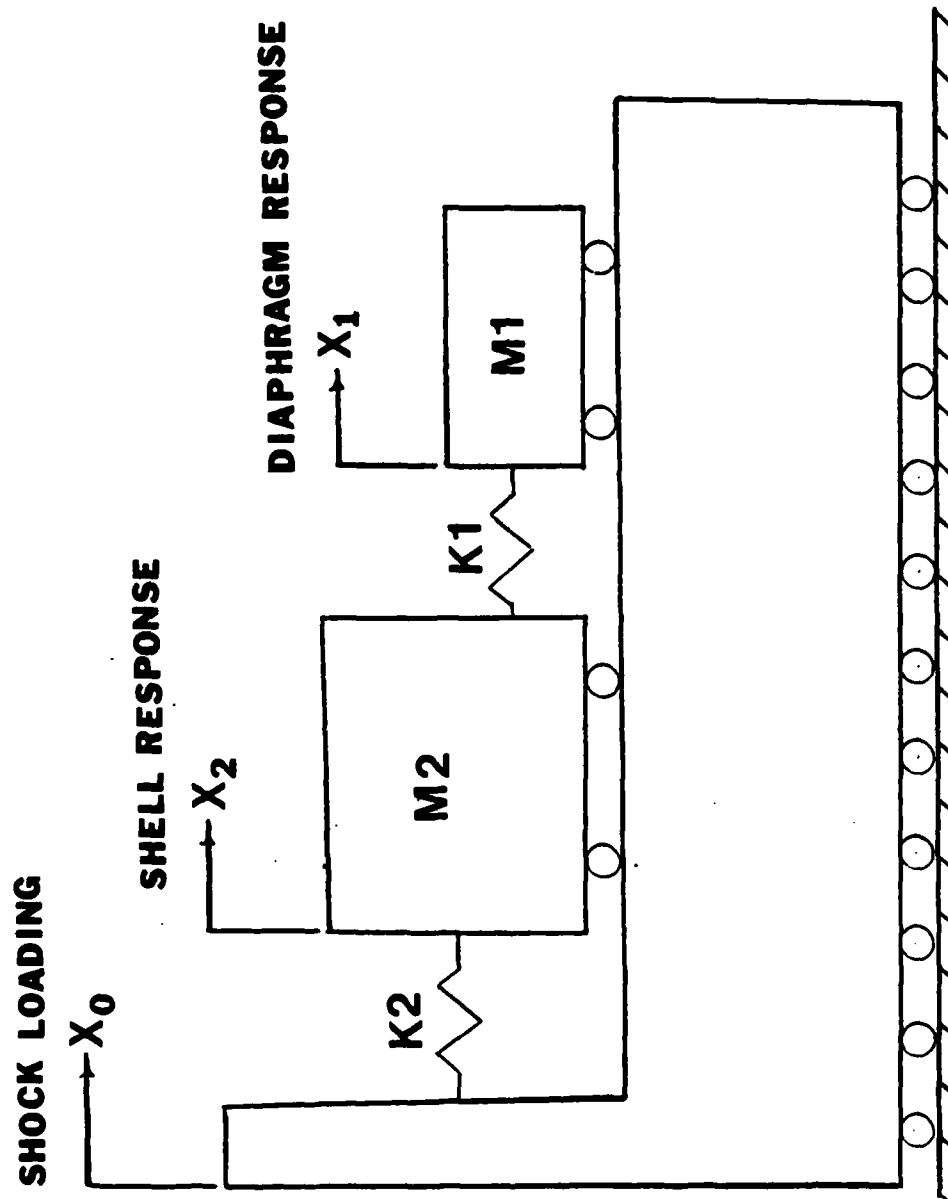


Figure 22. Two Degrees of Freedom System

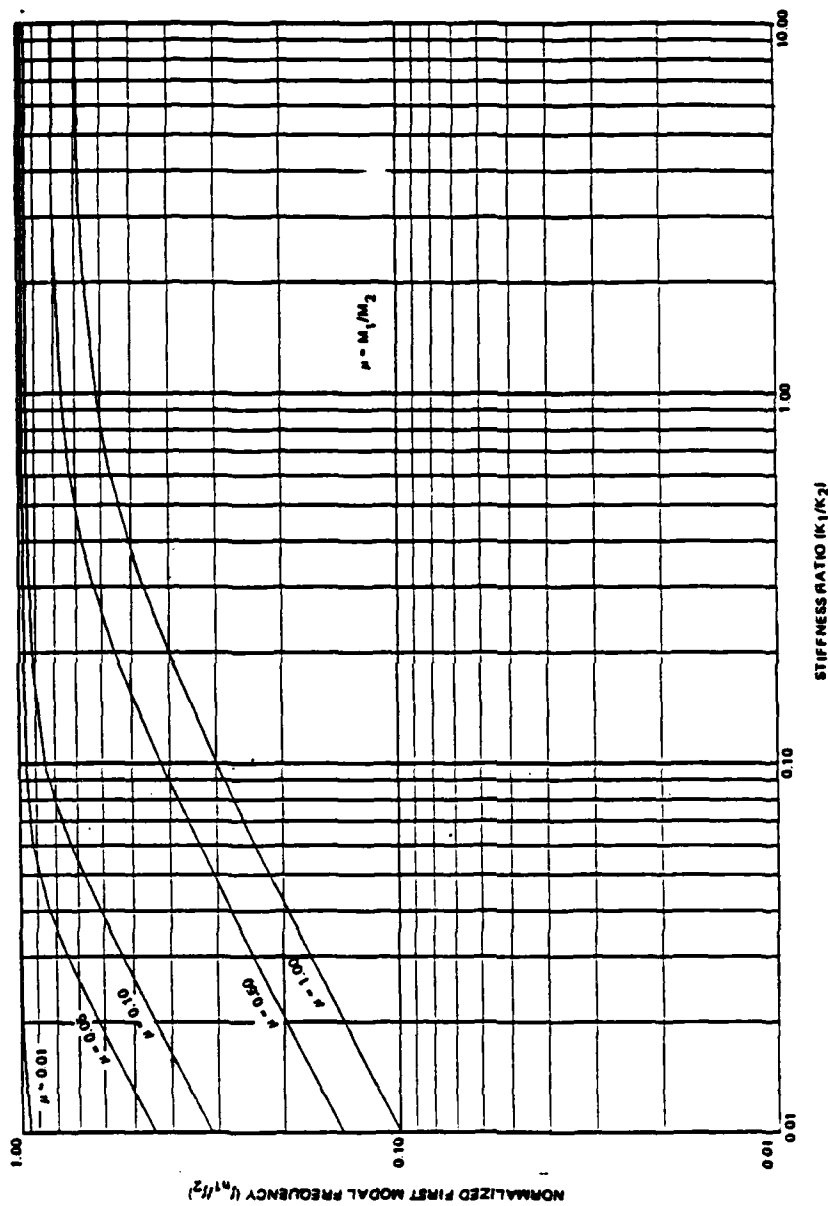


Figure 23. 2-DOF System First Modal Frequency vs. Stiffness Ratio for Various Mass Ratios [Ref. 12]

$$\omega = \bar{\omega} = \sqrt{K1/M1} = \sqrt{K2/M2} \quad (4)$$

where: $K1$ = overall stiffness of the substructure

$K2$ = overall stiffness of the shell

it can be said that:

$$K1/M1 = K2/M2 = K1/.08 M2$$

or

$$K1/K2 = .08$$

The coupled shell and substructure can then be modeled as a two degrees of freedom system as shown in Figure 22 where $M1$ and $K1$ represent the substructure and $M2$ and $K2$ represent the shell. The large mass ($M2$) has an uncoupled natural frequency (f_2) which is equal to $\sqrt{K2/M2}$. This is equivalent to the dominant frequency ($\bar{\omega}$) of the empty shell. Since this is a two degrees of freedom system, it will possess two natural frequencies for the coupled system. It has been found in coupled systems that for decreasing mass ratio ($M1/M2$) and for increasing stiffness ratio ($K1/K2$), the first and second modal frequencies of a two degrees of freedom system approach the decoupled frequencies f_1 and f_2 of two single degrees of freedom systems, respectively [Ref. 12]. The first natural frequency is bounded by f_2 , and f_1 is bounded by the second natural frequency. From Figure 23, it is seen that with $M1/M2 = K1/K2 = .08$, the dominant

frequency of the shell is approximately equal to the first modal frequency (f_{n1}) of the system. The result is that the shell/substructure system achieves resonance when excited at the dominant frequency of the empty shell.

With the diaphragm at resonance, Figures 24 and 25 illustrate that the transient response of the diaphragm is much more pronounced than that of the shell due to the large differences between the two masses as well as the soft spring between them. Initially the diaphragm is drawn in the negative X-direction by inertial forces as the shell is displaced by the shock wave. With the increased motion of the shell at frame nine, the diaphragm receives more and more energy. At approximately $t = 20$ msec, the diaphragm is at its maximum velocity while the shell is relatively calm. At this point, the diaphragm begins to transfer energy back to the shell. Since kinetic energy is equal to $1/2 MV^2$, the diaphragm is a small mass with high velocity while the much larger mass of the shell moves at a lower velocity. The energy of the system is transferred between the shell and substructure as the overall motion is damped by interaction between the shell and the fluid medium. The transfer of energy between the shell and the diaphragm creates an effect known as the "beating" phenomenon. This effect is seen in the velocity time history responses for the case of diaphragm resonance in Figures 26 through 39. The effect is

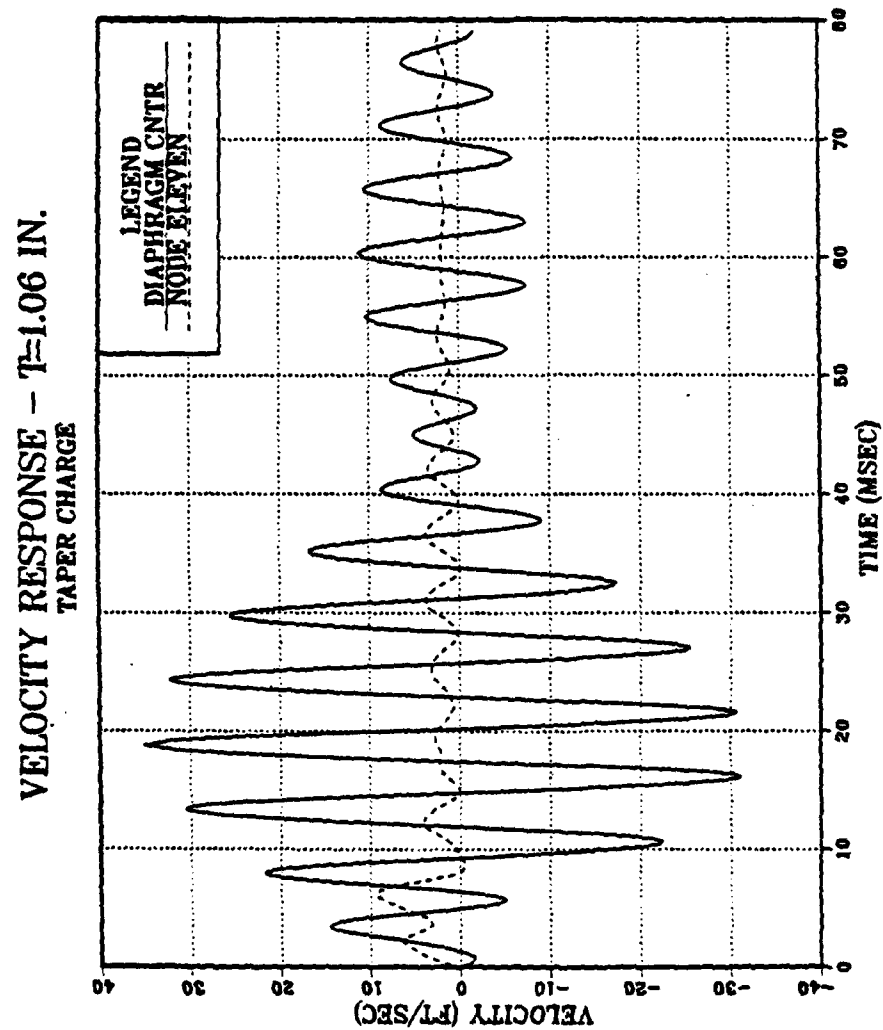


Figure 24. Energy Exchange Between Shell and Diaphragm (Taper Charge)

VELOCITY RESPONSE - $T=1.06$ IN.
CONVENTIONAL CHARGE

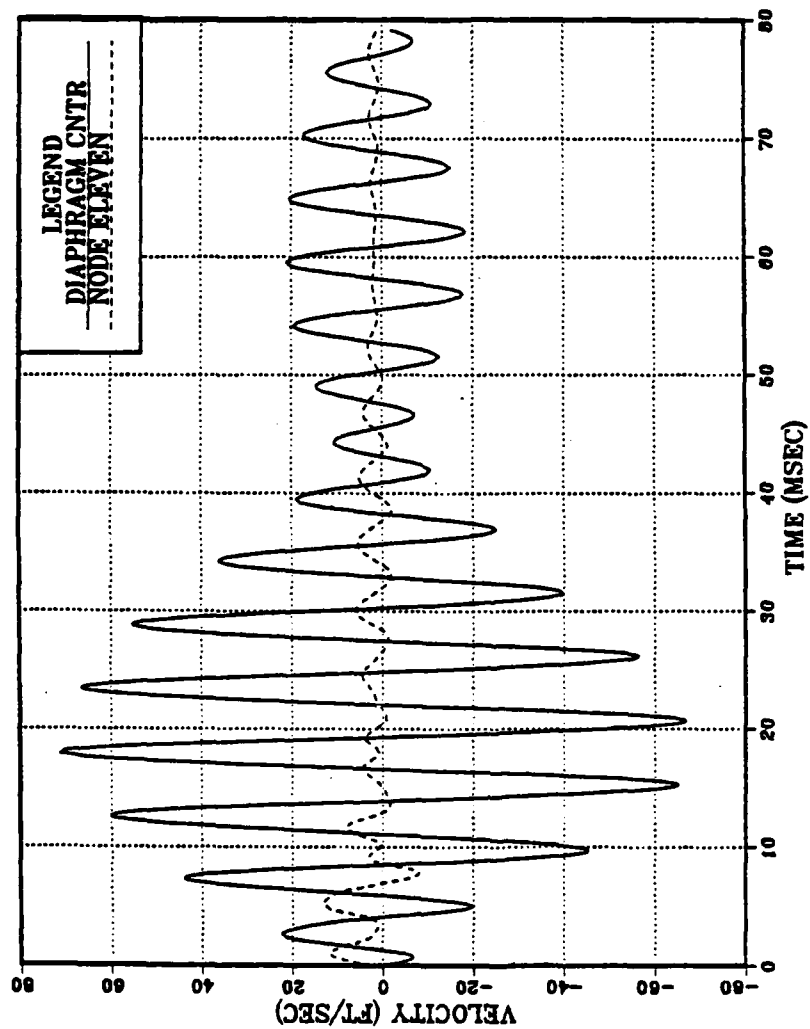


Figure 25. Energy Exchange Between Shell and Diaphragm (Conventional Charge)

VELOCITY RESPONSE - $T=1.06$ IN.

SEGMENT ONE - NODE ONE

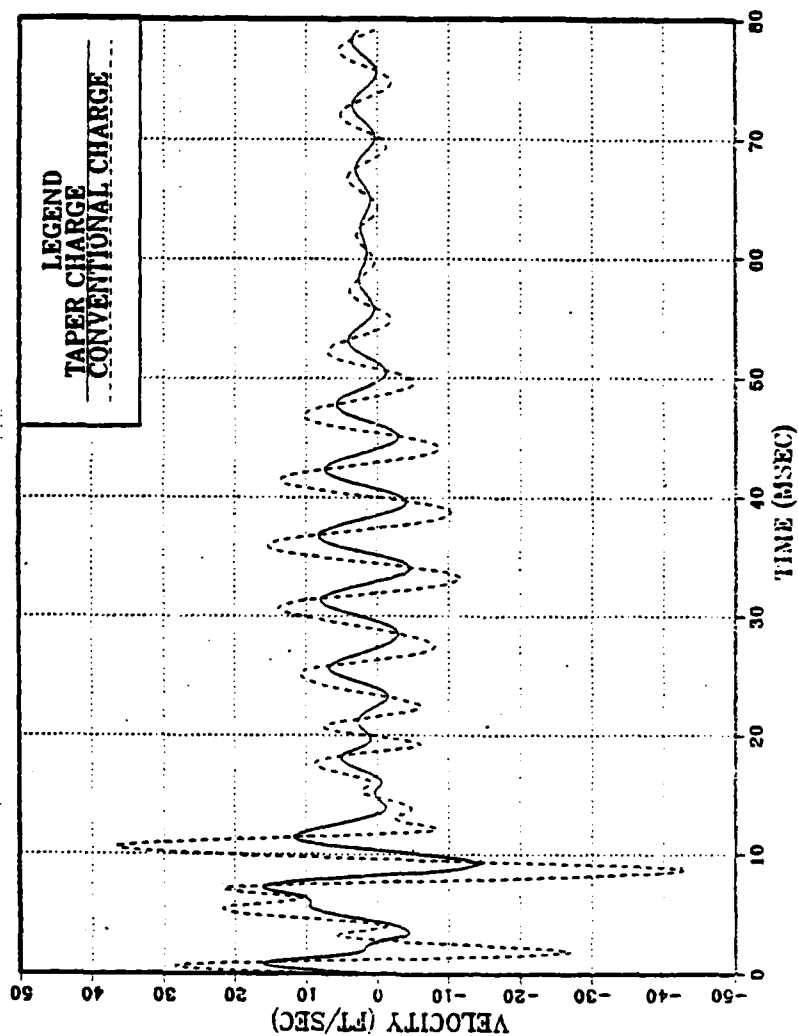


Figure 26. Velocity-Time History Response (Resonant Case) --FWD Endplate Center

VELOCITY RESPONSE - $T=1.06$ IN. SEGMENT TWO - NODE TWO

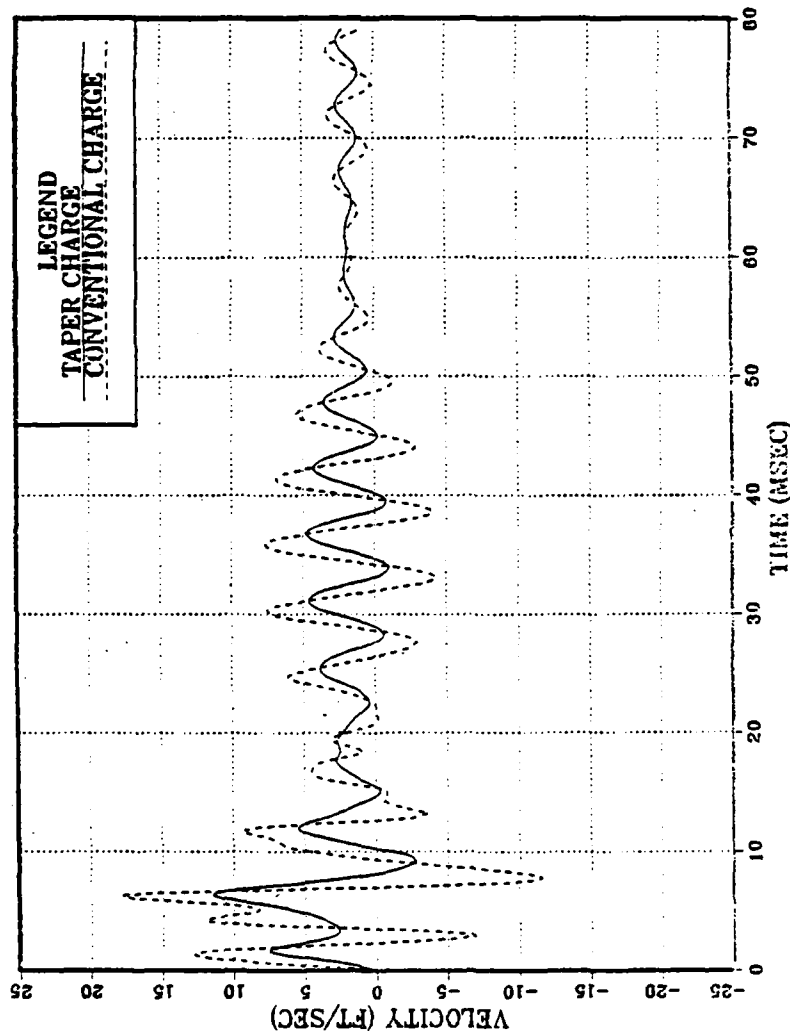


Figure 27. Velocity-Time History Response (Resonant Case) --Frame Zero

VELOCITY RESPONSE - $T=1.06$ IN.
SEGMENT TWO - NODE SEVEN

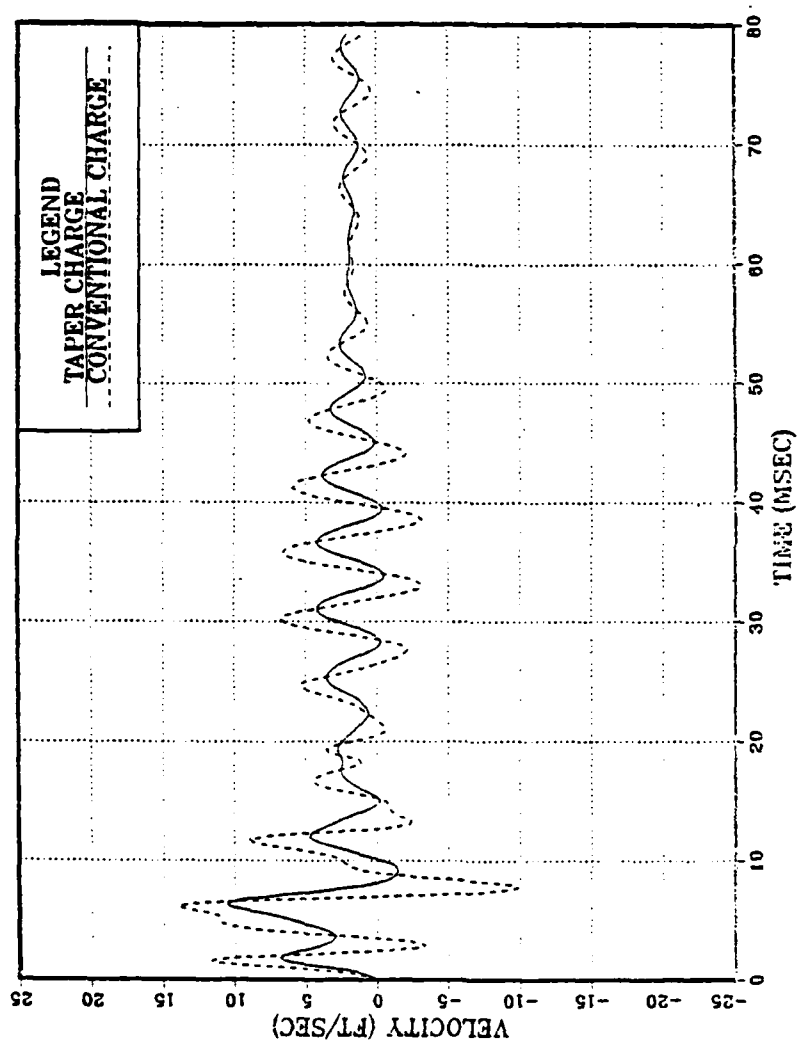


Figure 28. Velocity-Time History Response (Resonant Case) --Frame Five

VELOCITY RESPONSE - T=1.06 IN.
SEGMENT TWO - NODE ELEVEN

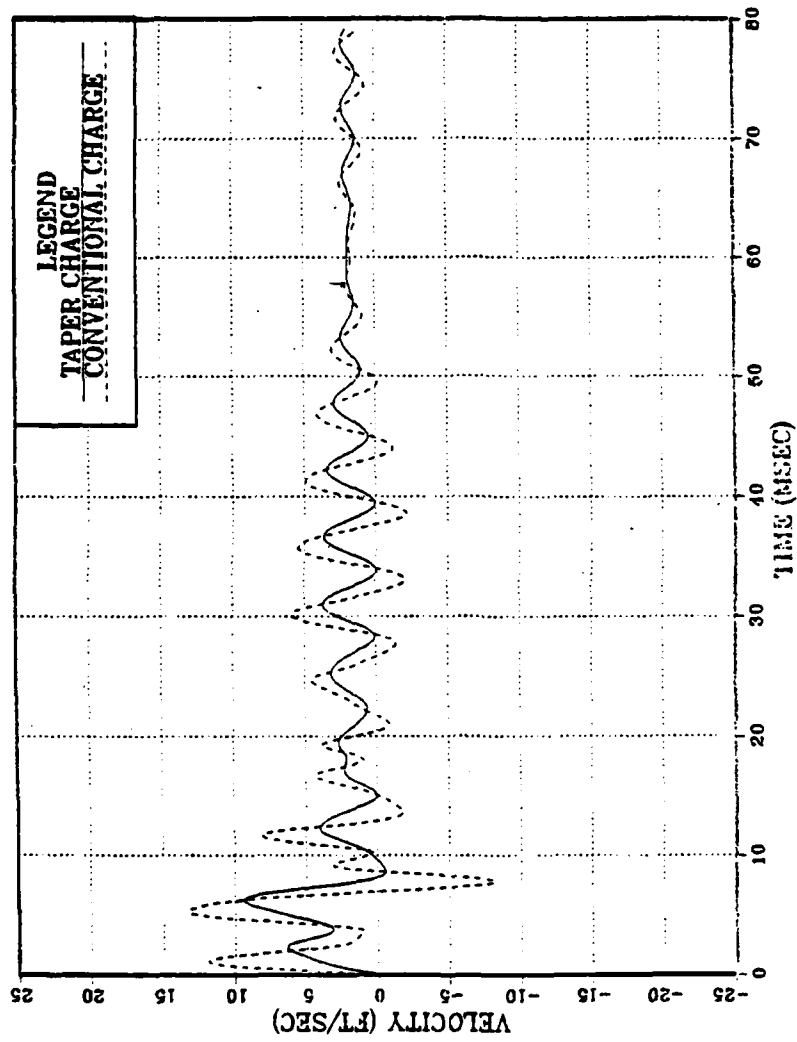


Figure 29. Velocity-Time History Response (Resonant Case) --Frame Nine

VELOCITY RESPONSE - $T=1.06$ IN.
DIAPHRAGM CENTER

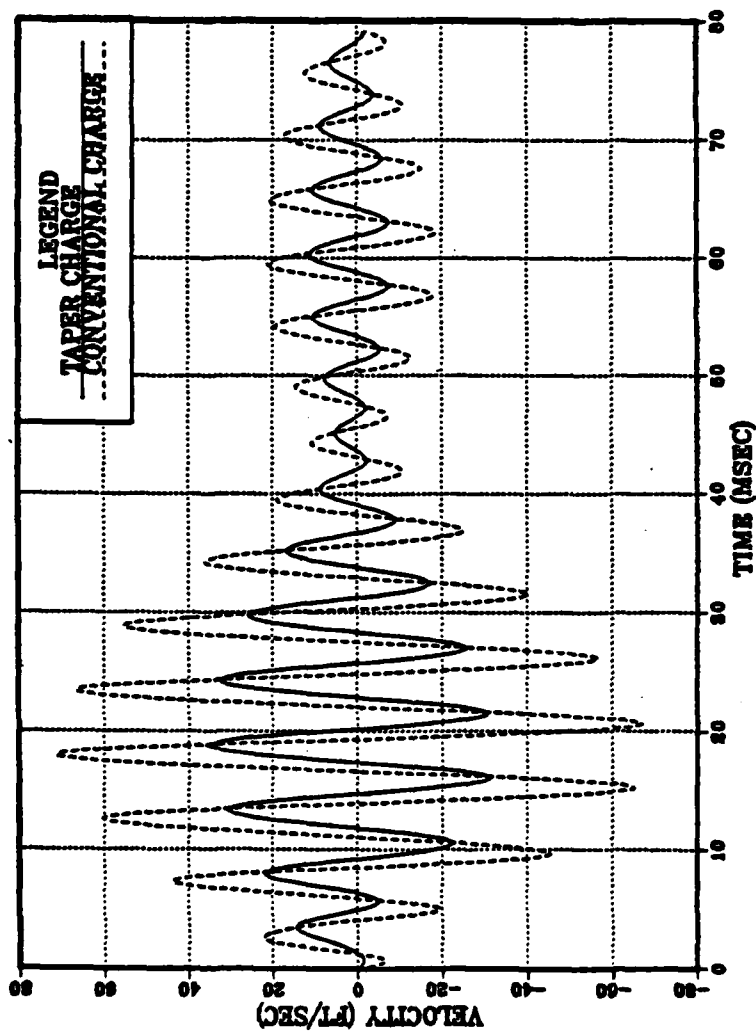


Figure 30. Velocity-Time History Response (Resonant Case) --Diaphragm Center

VELOCITY RESPONSE - T=1.06 IN.

SEGMENT TWO - NODE FIFTEEN

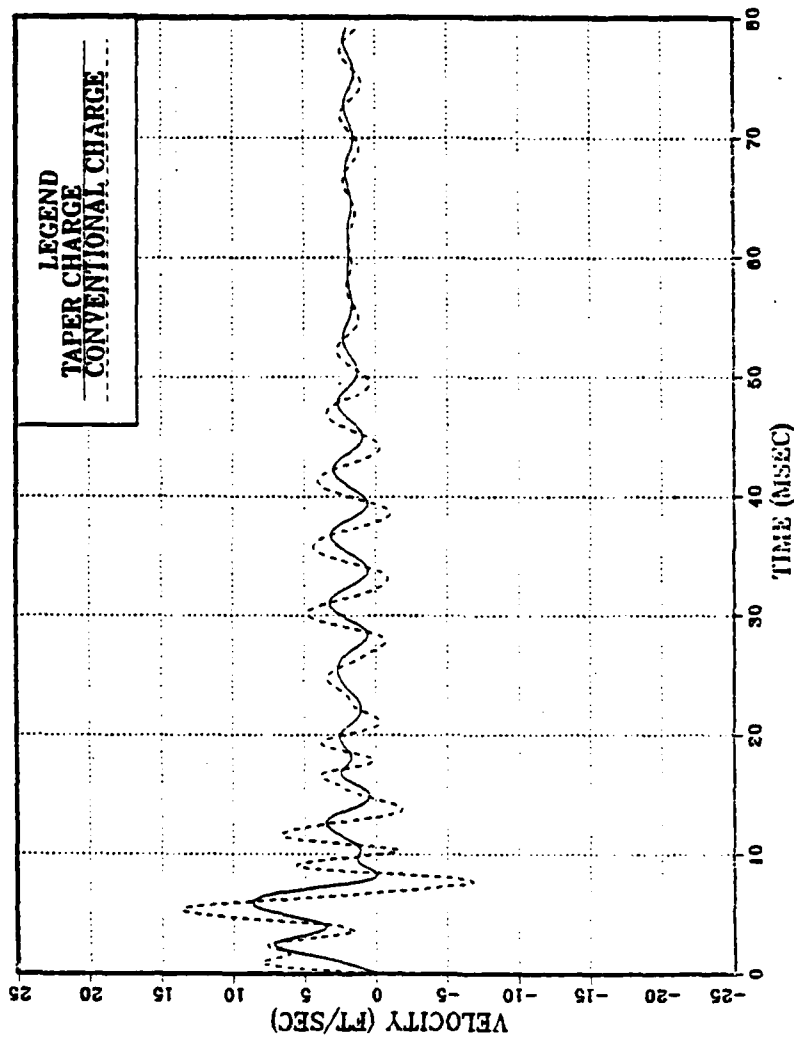


Figure 31. Velocity-Time History Response (Resonant Case) --Frame Thirteen

VELOCITY RESPONSE - $T=1.06$ IN.
SEGMENT TWO - NODE TWENTY

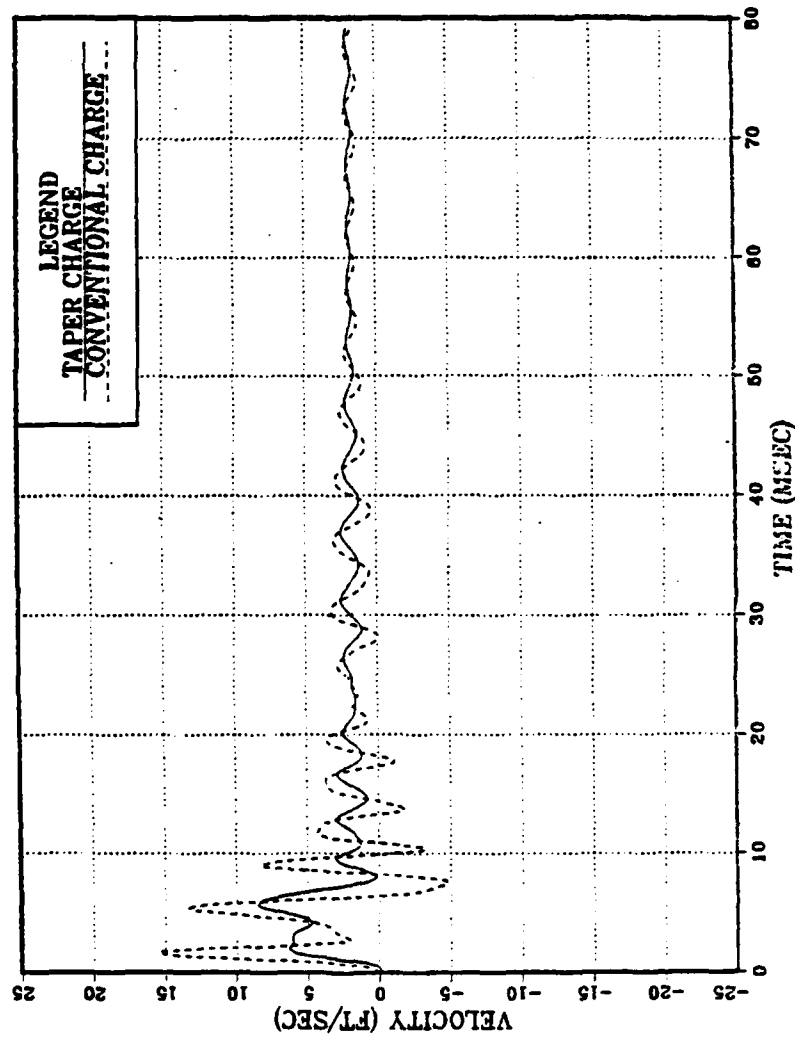


Figure 32. Velocity-Time History Response (Resonant Case) --Frame Eighteen

VELOCITY RESPONSE - $T=1.06$ IN.
SEGMENT TWO - NODE TWENTY FOUR

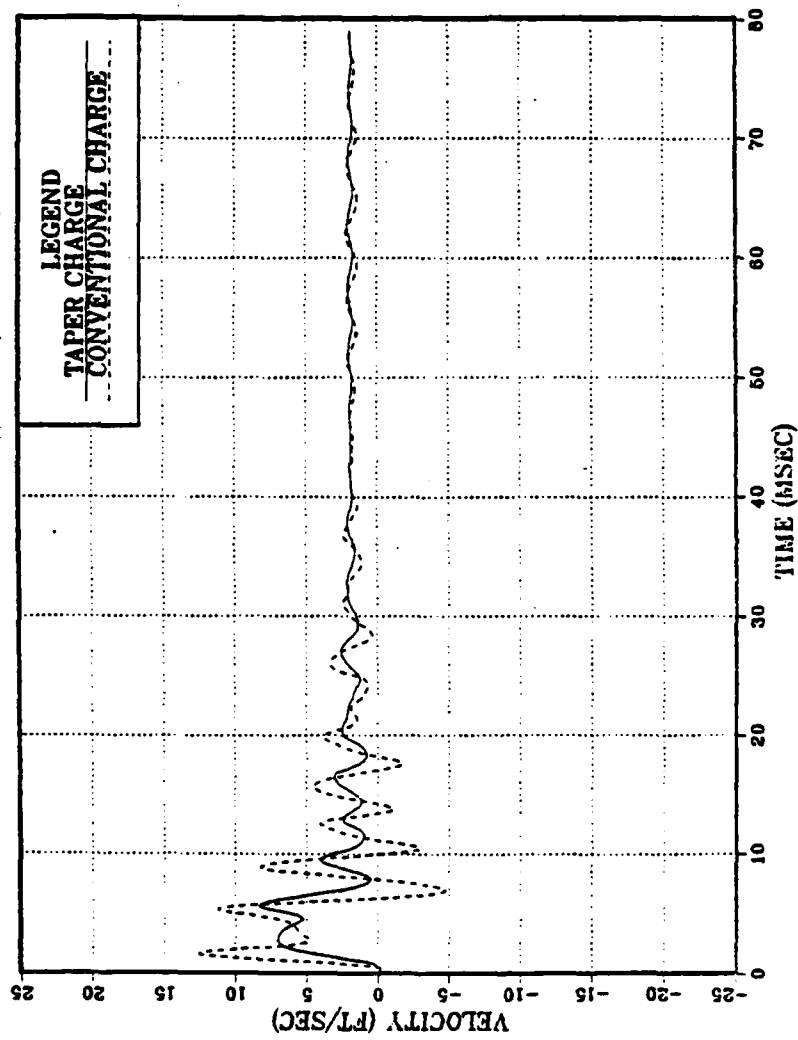


Figure 33. Velocity-Time History Response (Resonant Case) --Frame Twenty-Three

VELOCITY RESPONSE - T=1.06 IN.
SEGMENT TWO - NODE TWENTY EIGHT

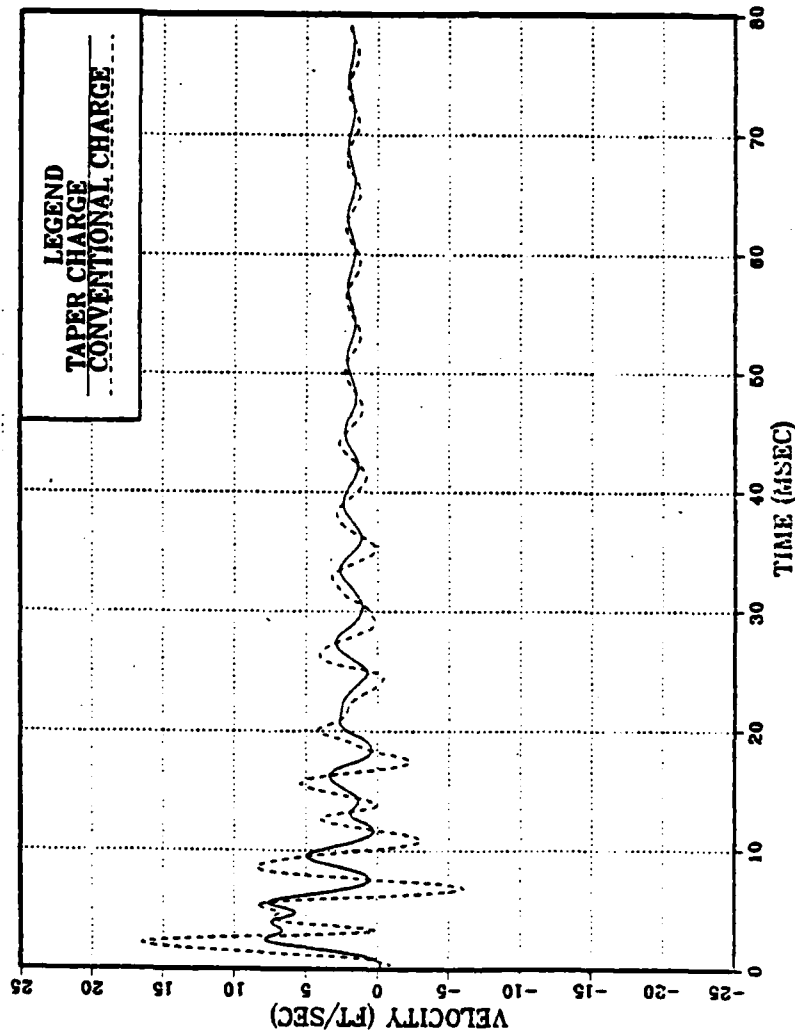


Figure 34. Velocity-Time History Response (Resonant Case) --Frame Twenty-Seven

VELOCITY RESPONSE - $T=1.06$ IN.
SEGMENT TWO - NODE THIRTY THREE

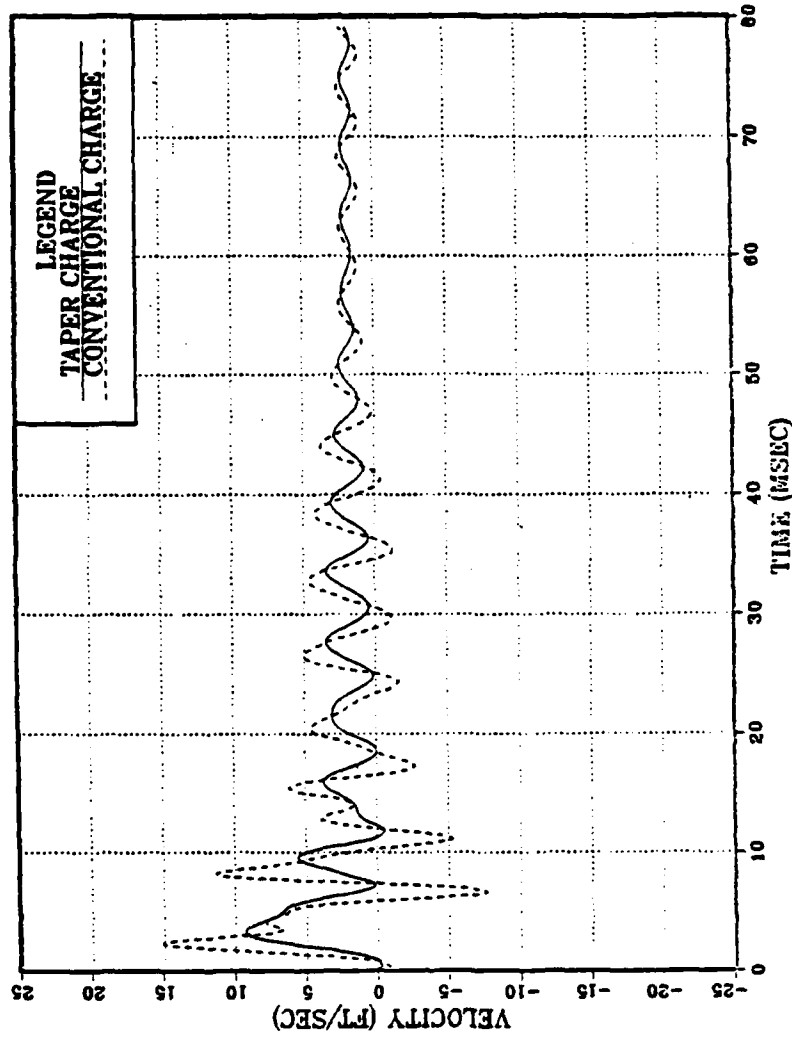


Figure 35. Velocity-Time History Response (Resonant Case) --Frame Thirty-Two

VELOCITY RESPONSE - $T=1.06$ IN.
SEGMENT TWO - NODE THIRTY SEVEN

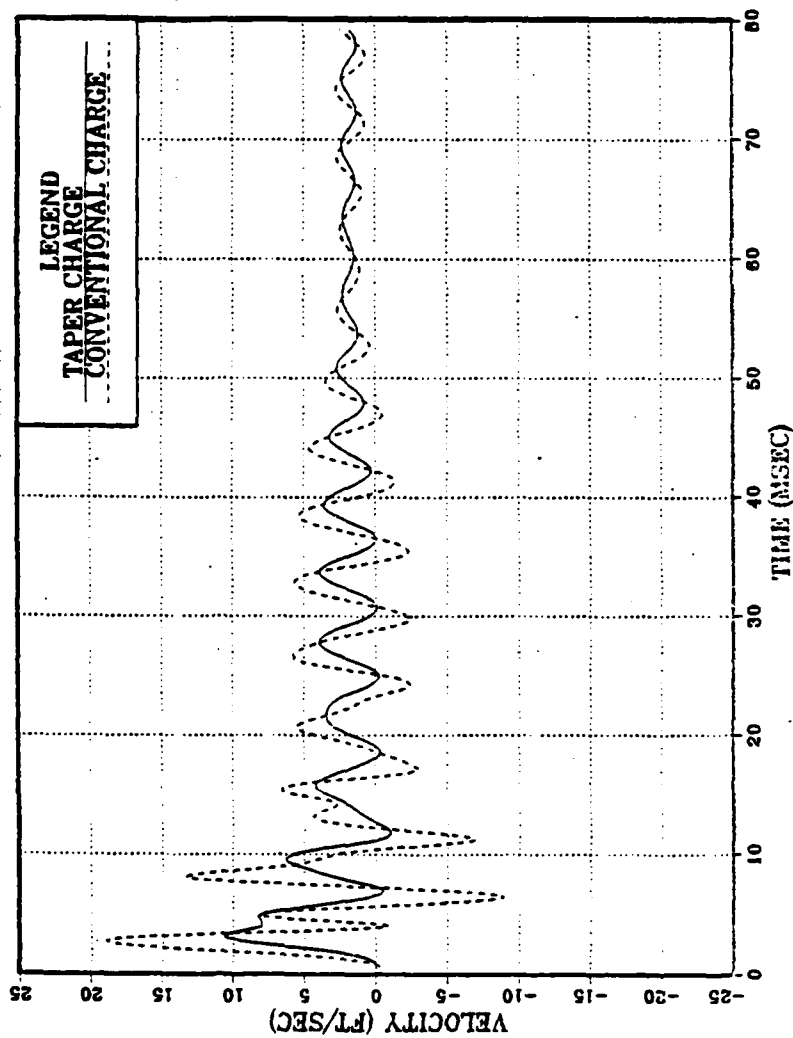


Figure 36. Velocity-Time History Response (Resonant Case) --Frame Thirty-Six

VELOCITY RESPONSE - $T=1.06$ IN.
SEGMENT TWO - NODE FORTY ONE

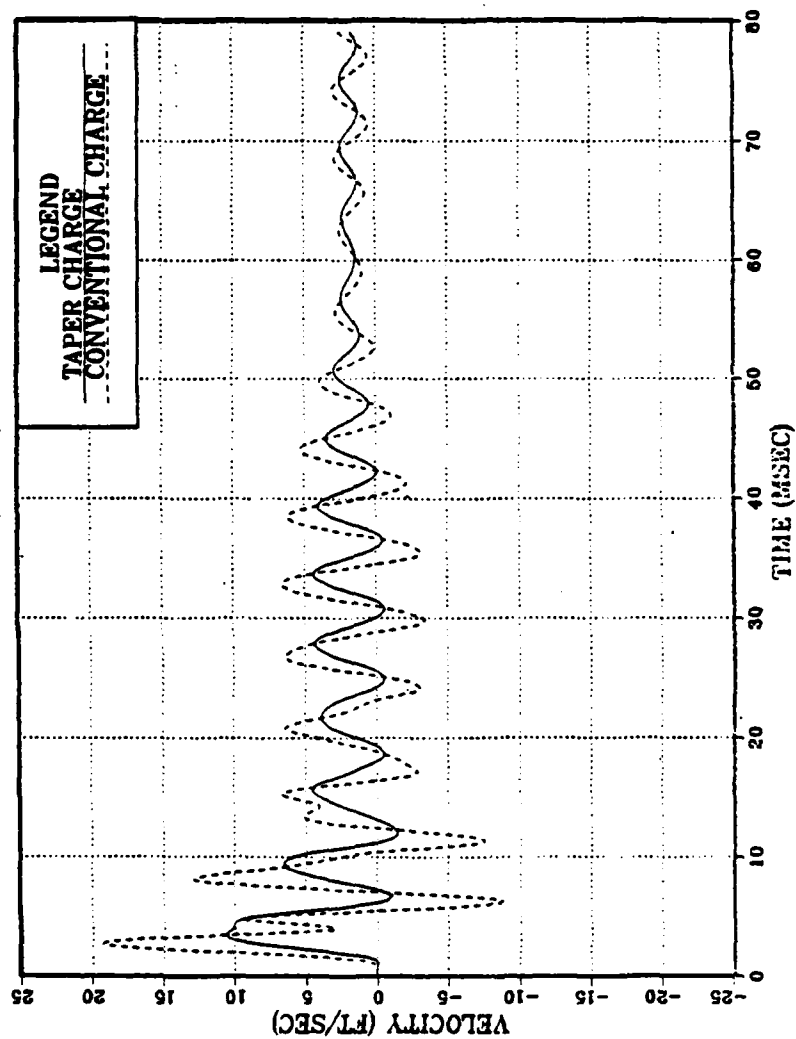


Figure 37. Velocity-Time History Response (Resonant Case) --Frame Forty

VELOCITY RESPONSE - $T=1.06$ IN.
SEGMENT TWO - NODE FORTY SIX

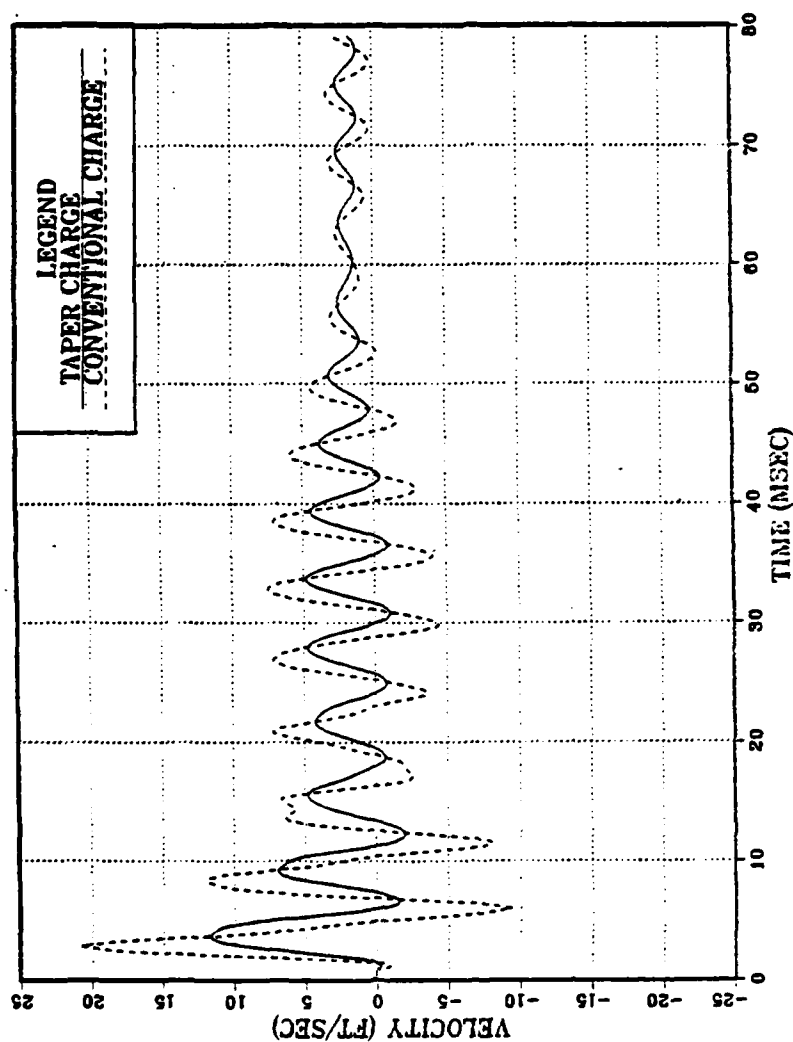


Figure 38. Velocity-Time History Response (Resonant Case) --Frame Forty-Five

VELOCITY RESPONSE - $T=1.06$ IN.
SEGMENT THREE - NODE TWELVE

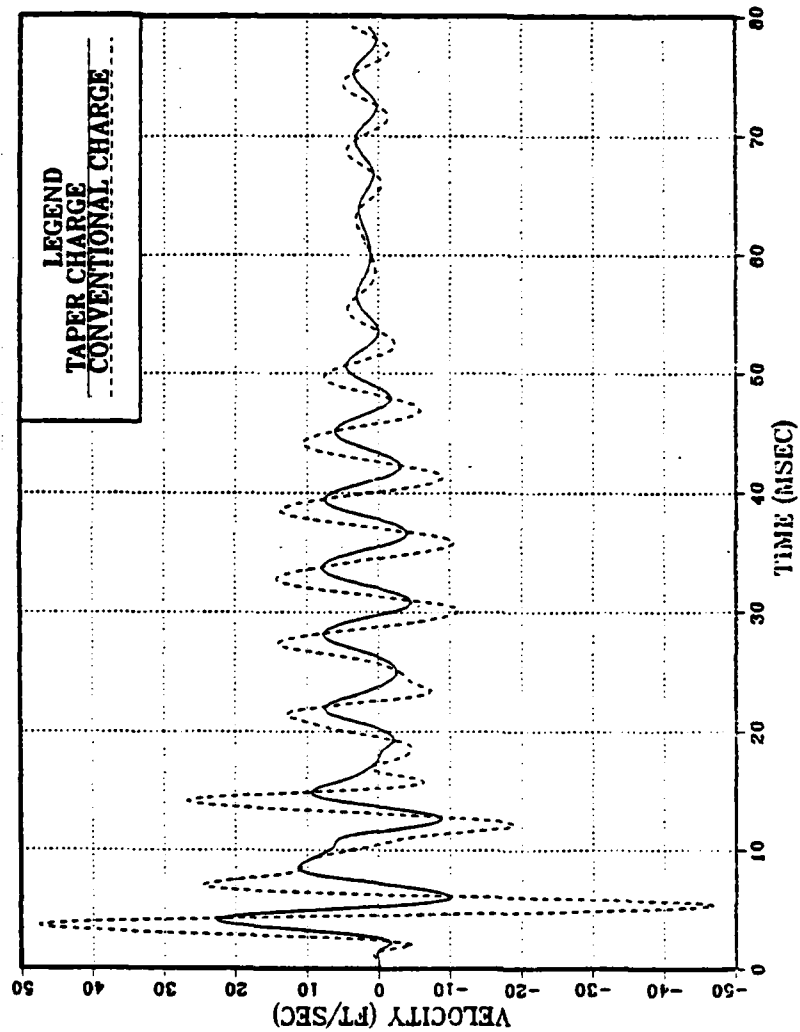


Figure 39. Velocity-Time History Response (Resonant Case) --AFT Endplate Center

quite pronounced at the endplates, because they act as "hard spots" receiving the energy transmitted through the shell. The cylindrical portion of the shell acts as a conduit for the energy transfer. Again, the nodes on the shell nearest the endplate experience some local deformation due to the rigid coupling between segments.

The empty shell velocity-time history response is compared with the resonant diaphragm case in Figures 40 through 45. Of particular interest is the fact that the velocity profiles are virtually identical for the first fifteen milliseconds. During this period of time, the shell is receiving energy from the shock wave and transferring a portion of it to the diaphragm. Because of the differences in mass between the shell and substructure, not much energy is lost from the shell. The peak velocities do not vary by more than five feet per second during this time period. The difference arises at $t = 35$ msec when the shell receives energy from the resonating plate. The decaying velocity response is disturbed during the exchange of energy which is observed in the beating effect.

As the thickness of the diaphragm is increased beyond the resonant condition, the interactions between the shell and substructure are reduced dramatically. The shell/substructure velocity-time history remains within 10% of the empty shell response until the diaphragm thickness is 2.25

EMPTY SHELL VS. T=1.06 IN. SEGMENT ONE - NODE ONE

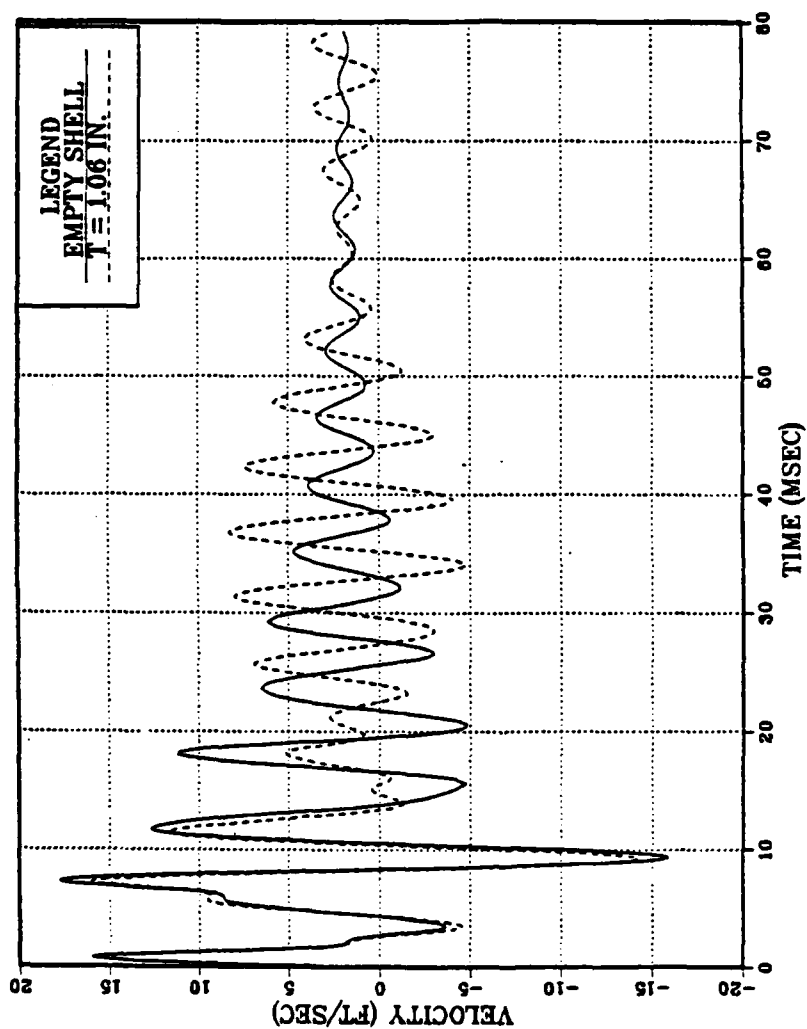


Figure 40. Comparison of Empty vs. Resonant Shell Response (Taper Charge)--Forward Endplate Center

EMPTY SHELL VS. $T=1.06$ IN. SEGMENT TWO - NODE ELEVEN

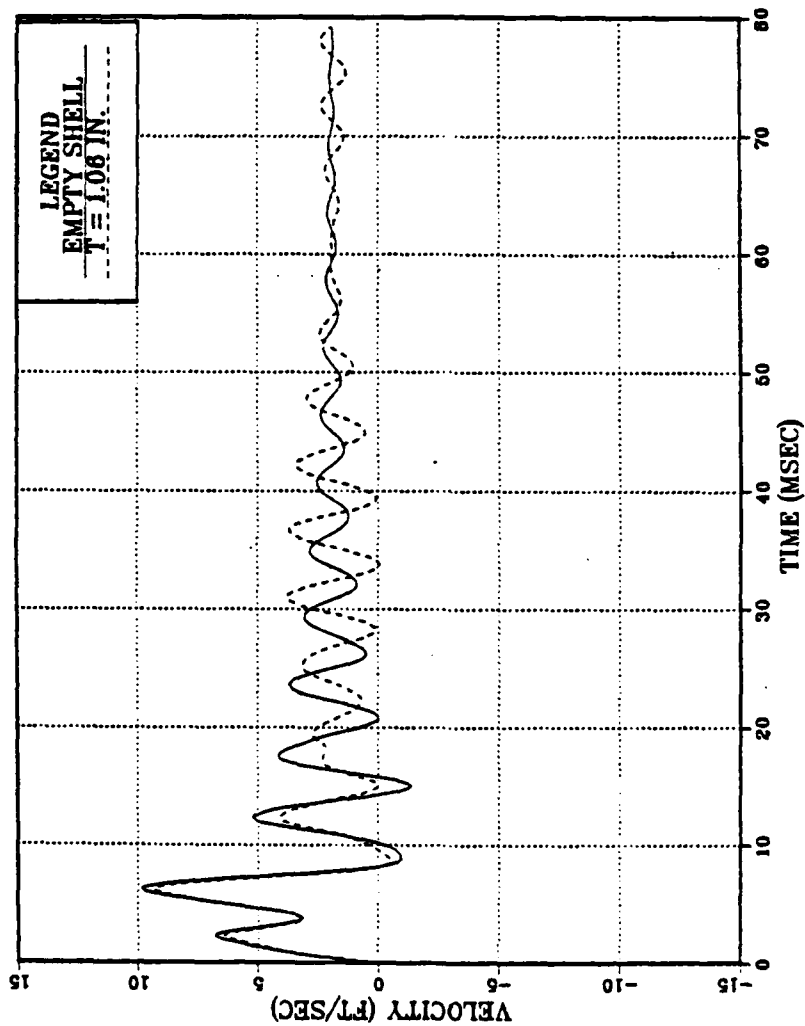


Figure 41. Comparison of Empty vs. Resonant Shell Response (Taper Charge) --Frame Nine

EMPTY SHELL VS. $T=1.06$ IN. SEGMENT THREE - NODE TWELVE

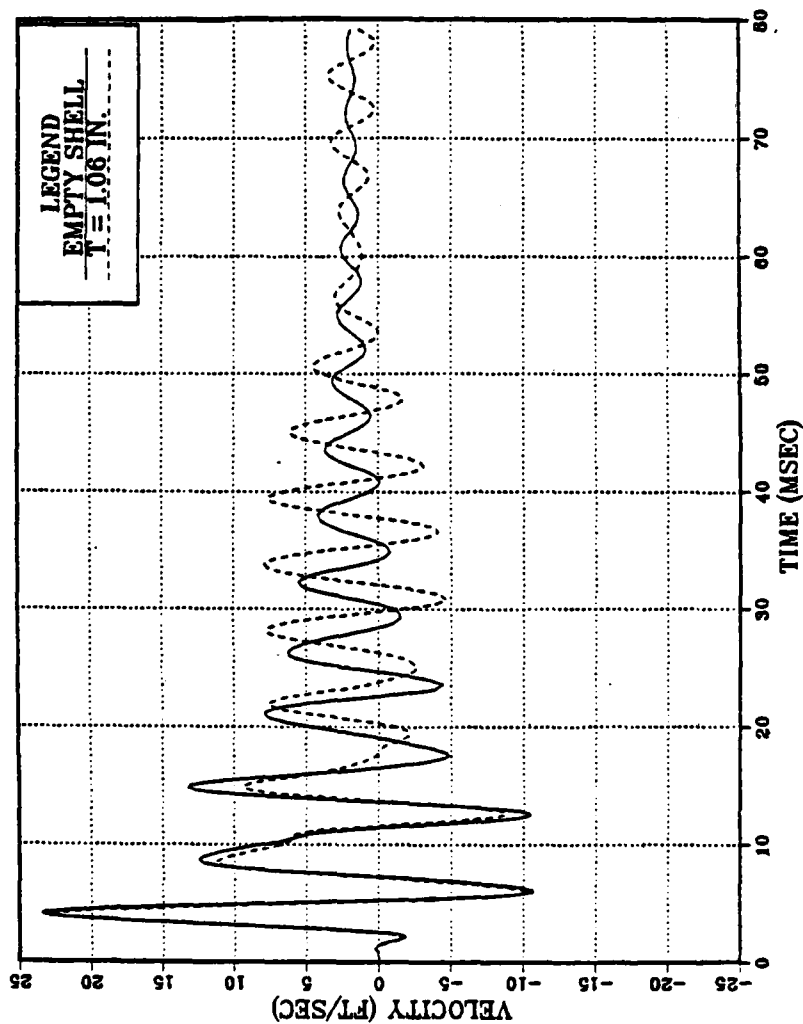


Figure 42. Comparison of Empty vs. Resonant Shell Response (Taper Charge) --AFT Endplate Center

EMPTY SHELL VS. T=1.06 IN. SEGMENT ONE - NODE ONE

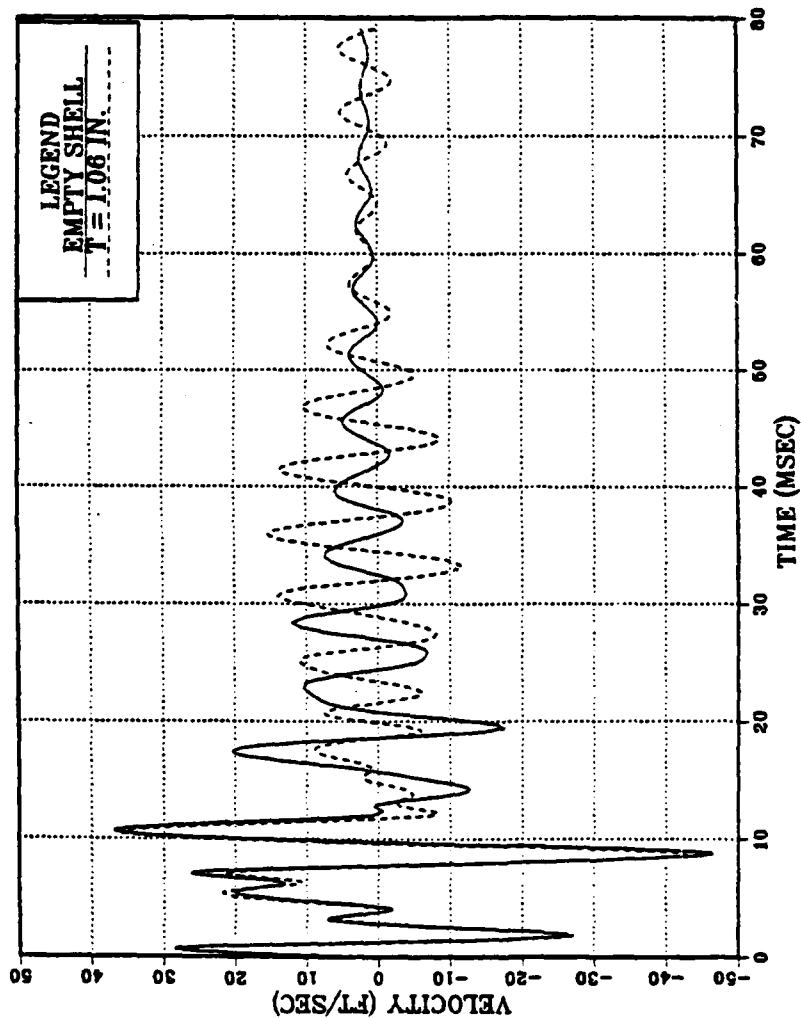


Figure 43. Comparison of Empty vs. Resonant Shell Response (Conventional Charge) -- Forward Endplate Center

EMPTY SHELL VS. $T=1.06$ IN.
SEGMENT TWO - NODE ELEVEN

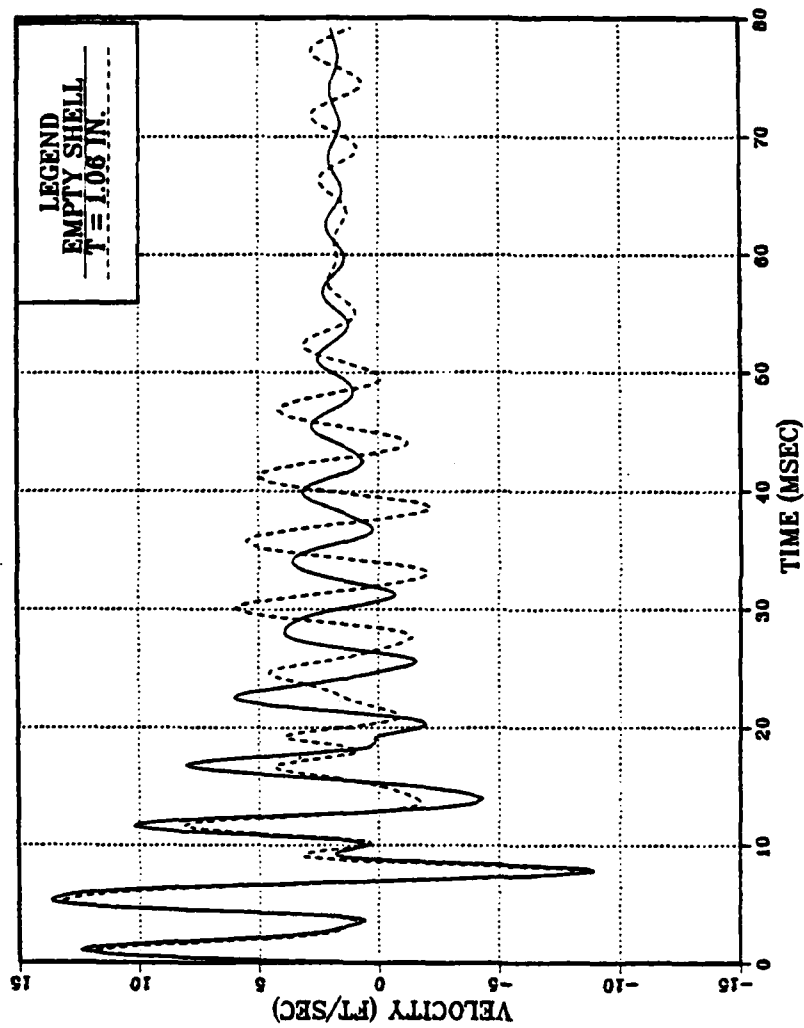


Figure 44. Comparison of Empty vs. Resonant Shell Response (Conventional Charge) --
Frame Nine

EMPTY SHELL VS. $T=1.06$ IN.
SEGMENT THREE - NODE TWELVE

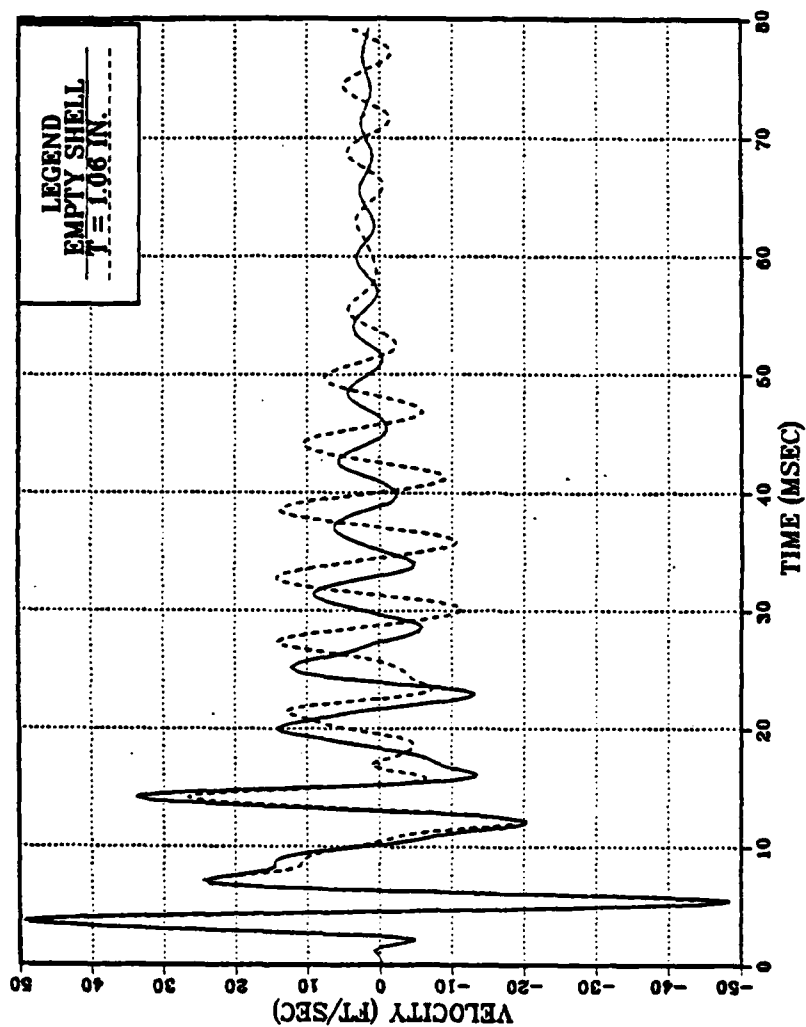


Figure 45. Comparison of Empty vs. Resonant Shell Response (Conventional Charge) --
AFT Endplate Center

inches thick or $M1/M2 = .164$. By the time it is 9.25 inches thick, it represents over half the mass of the shell, and it acts as if it was an integral part of the shell slaved to the motions of the forward endplate.

VI. CONCLUSIONS

Upon inspection of the velocity-time history responses at various locations along the shell, one can see why the potential for damage is so great from an underwater explosion off the bow or stern of a submarine. While the cylindrical portion for the most part serves to transmit inertial forces with little velocity response, the extremities of the hull experience violent transient responses which may be passed to attached internal equipment located in those areas. The inertial influence of the mass of the endplates on neighboring nodes of the shell is apparent in both the empty shell and resonant cases. The response from a conventional charge is seen to be much more pronounced than that of a taper charge of equivalent impulse due to the rapid expenditure of energy against the forward endplate.

The results obtained from the resonant diaphragm case support the theory that with decreasing mass ratio between substructure and shell, the first and second modal frequencies of the two degrees of freedom system approach the decoupled frequencies of the substructure and shell in two single degree of freedom systems. This allows the motion of hull to drive the diaphragm into resonance when

the dominant frequency of the shell motion is roughly equal to the fundamental frequency of the substructure. It is possible that this could occur during an underwater shock test of a small piece of equipment in a large SSTV. This might result in the failure of the equipment in a scenario which would not occur in a real submarine with its myriad of internal masses and substructures.

The large difference in mass between the substructure and the shell results in a tremendous dynamic amplification in the response of the diaphragm at resonance. As energy is transferred between the two bodies, the large mass of the shell causes its velocity to be quite small compared to that of the diaphragm. As is seen in Figures 40 through 45, the initial resonant case velocity response is virtually unchanged from the empty shell response. If the mass of the internal equipment was sufficiently small in comparison to an SSTV used in a series of shock tests, one ELSHOK calculation could be performed on the empty shell to generate a set of velocity response curves. The velocity-time history response at the attachment point could then be input into the SAPIV code for the finite element model of any number of small pieces of equipment, and the substructure transient response could be obtained without having to run a separate ELSHOK calculation for each shell/substructure system. This would result in considerable savings in computer time.

Although ELSHOK is a powerful tool which can be used to accurately predict the results of underwater explosion tests on equipment, some shortfalls exist in the program which limit its use in design applications. At the present time, there is no direct method to take the effects of the surface cut-off wave or bottom reflection into account. The surface cut-off wave forms in shallow underwater explosions when the compressive shock wave reflects off of the surface of the water causing a tensile wave to propagate. Bottom reflections form in deep explosions as the shock wave is reflected off of the floor of the ocean. ELSHOK assumes that the explosion is occurring in an infinite acoustic medium with a single shock wave. Another weakness in the program is the fact that it cannot process oblique explosions; charges must be placed in a pure end-on or side-on configuration. Shock tests conducted in accordance with MIL-S-901D are either end-on or side-on loading, however, so this is not a serious drawback in predicting the transient motion of equipment in SSTV's.

It is recommended that further study be conducted in this area using more refined shell models resembling full-scale submarines. Once a shell model is produced for a given submarine class, researchers can create different finite element models of actual equipment to observe the interactions between the submarine hull and equipment of

varying mass and shape when subjected to end-on or side-on loads. It is felt that ELSHOK is an effective method to give an indication of the response of equipment in underwater explosion tests without needless destruction from unexpected failures. Its continued use prior to UNDEX tests will lead to savings in both time and effort.

LIST OF REFERENCES

1. Department of the Navy Military Specification MIL-S-901D (Navy), Shock Tests, H.I. (High Impact) Shipboard Machinery, Equipment, and Systems, Requirements for, 20 October 1978.
2. Geers, T. L., "Residual Potential and Approximate Methods for Three-Dimensional Fluid-Structure Interaction Problems," Journal of the Acoustical Society of America, V. 49, No. 5 (Part 2), pp. 1505-1510, 1971.
3. Welch, M. S., Numerical Analysis of the Elastic Shock Response of Submarine Installed Equipment, Master's Thesis, Naval Postgraduate School, Monterey, California, September 1984.
4. Vasudevan, R. and Ranlet, D., Submerged Shock Response of a Linearly Elastic Shell of Revolution Containing Internal Structure: User's Manual for the ELSHOK Code, Weidlinger Associates, New York, New York, May 1982.
5. Ranlet, D., DiMaggio, F. L., Bleich, H. H., and Baron, M. L., "Elastic Response of Submerged Shells with Internally Attached Structures to Shock Loading," International Journal of Computers and Structures, V. 7, No. 3, pp. 355-364, June 1977.
6. Ranlet, D. and DiMaggio, F. L., "Transient Response of Shells with Internally Attached Structures," International Journal of Computers and Structures, V. 9, No. 5, pp. 475-481, November 1978.
7. Bushnell, D., Stress, Stability and Vibration of Complex Branched Shells of Revolution: Analysis and User's Manual for BOSOR4, LSMC-D 243605 Lockheed Missiles and Space Company, Inc., Sunnyvale, California, March 1972.
8. Earthquake Engineering Research Center Report No. EERC 73-11, SAPIV-A Structural Analysis Program for Static and Dynamic Response of Linear Systems, by K. J. Bathe, E. L. Wilson, and F. E. Peterson, University of California, Berkeley, California, April 1974.

9. Cole, R. H., Underwater Explosions, pp. 228-269, Princeton University Press, 1948.
10. Little, R., Elasticity, p. 279, Prentice-Hall, Inc., 1973.
11. Butt, L., Naval Ship Shock Design and Analysis, Lecture notes presented at Naval Postgraduate School, ME 4525, Spring 1985.
12. Shin, Y. S., Effects of Undesigned for High-Frequency Vibrations on Plant Equipment Components, NEDE-25494, General Electric Company, San Jose, California, December 1981.

APPENDIX A

PROGRAM USED TO CONVERT PUSLOB PUNCH CARD FILES TO FORMAT ACCEPTANCE BY EASYPLOT

Along with the TEKTRONIX plots of the velocity-time histories, PUSLOB generates velocity punch card files for each requested node. The punch card file consists of a block of velocities in exponential format the size of which depends upon the number of time points requested. The EASYPLOT program developed for the IBM 3033 by Mr. John Mainwaring is a quick interactive method to produce graphs using DISSPLA without having to create a plotting program. It will accept up to 100 data points in tabular form provided it is in a column format for X-Y input. The PLOTCONV1 code was created to accept data from two separate punch card files for taper and conventional charge comparisons and combine them into one data file for each node for input into EASYPLOT.

In order to prevent data overflow, the time step must be sized in USLOB and PUSLOB to generate no more than 100 velocity data points. Both the PLOTCONV1 VAX 11/780 VMS computer command file and the FORTRAN code are included in this appendix. The command file must be modified prior to each run to specify the punch card files being read and the titles of the new data files.

```

$! PLOTCONV1.COM - - COMMAND FILE FOR EXECUTION OF PLOTCONV1
$!
$ ASSIGN PUSL48.PUN FOR011
$ ASSIGN PUSL49.PUN FOR012
$ ASSIGN MAXSHL1.DAT FOR021
$ ASSIGN MAXSHL2.DAT FOR022
$ ASSIGN MAXSHL3.DAT FOR023
$ ASSIGN MAXSHL4.DAT FOR024
$ ASSIGN MAXSHL5.DAT FOR025
$ ASSIGN MAXSHL6.DAT FOR026
$ ASSIGN MAXSHL7.DAT FOR027
$ ASSIGN MAXSHL8.DAT FOR028
$ ASSIGN MAXSHL9.DAT FOR029
$ ASSIGN MAXSHL10.DAT FOR030
$ ASSIGN MAXSHL11.DAT FOR031
$ ASSIGN MAXSHL12.DAT FOR032
$ ASSIGN MAXSHL13.DAT FOR033
$ ASSIGN MAXSHL14.DAT FOR034
$!
$ RUN PLOTCONV1
$!

```

PROGRAM PLOTCONV1

C
C
C
C
C

THE PURPOSE OF THIS PROGRAM IS TO READ TWO PUNCH-CARD
FILES FROM PUSLOB AND CONVERT THEM TO A FORMAT WHICH CAN
BE ACCEPTED BY EASYPLOT.

```

      DIMENSION VEL(100,14),VELO(100,3),VEL1(100,14),LABEL(14),TAG(14),
      %LTITLE(14)
      CHARACTER*10 LABEL
      CHARACTER*40 LTITLE
      COMMON/CSOLVE/DTRECS
      NCURV=14
      DO 10 K=1,NCURV
      READ(11,999) LTITLE(K),NRECS,DTRECS
      READ(11,998) LABEL(K),TAG(K)
      READ(11,997) (VEL(J,K),J=1,NRECS)
      READ(12,999) LTITLE(K),NRECS,DTRECS
      READ(12,998) LABEL(K),TAG(K)
      READ(12,997) (VEL1(J,K),J=1,NRECS)
10    CONTINUE
999  FORMAT(A40,I5,1PE11.4)
998  FORMAT(A10,F10.5)
997  FORMAT(1P7E11.4)
      DO 20 L=1,NCURV
      T=0.0
      LL=L+20
      DO 30 M=1,NRECS
      VELO(M,1)=T
      DTRECS1=1000.0*DTRECS
      T=T+DTRECS1
      VELO(M,2)=VEL(M,L)/12.0
      VELO(M,3)=VEL1(M,L)/12.0
30    CONTINUE
      DO 40 KK=1,NRECS
      WRITE(LL,996) (VELO(KK,JJ),JJ=1,3)
40    CONTINUE
      WRITE(LL,995) LTITLE(L),NRECS,DTRECS
      WRITE(LL,994) LABEL(L),TAG(L)
20    CONTINUE
996  FORMAT(3F15.5)
995  FORMAT(A40,I5,1PE11.4)
994  FORMAT(A10,F10.5)
      STOP

```

APPENDIX B

TYPICAL ELSHOK INPUT CODES--SHELL AND SUBSTRUCTURE

The input codes which follow are for the resonant diaphragm case for both taper and conventional charges. The only differences between the two is in the USLOB code where the type of charge is specified. All the input codes are explained in detail in the ELSHOK users manual [Ref. 4].

1. BOSOR4 INPUT DATA

The BOSOR4 input code is created by working interactively with the computer. The prompt following the \$ symbol appears, and the user supplies the required information. The three segments (two endplates and cylinder) are modeled separately, and then they are "connected" in the global data section. A separate input code is required for each circumferential harmonic included in the calculation. BOSOR4 output provides the user with the in-vacuo free-free modes and natural frequencies of the shell.

AD-A167 887

A PARAMETRIC STUDY OF ELASTIC RESPONSES OF
SUBMARINE-INSTALLED EQUIPMENT. (U) NAVAL POSTGRADUATE
SCHOOL MONTEREY CA S A WEINHARDT MAR 86

2/2

UNCLASSIFIED

F/G 13/10.1 NL





MICROCOPY

CHART

FILE: BOSSO DATA A1

```

OSOR4 ATTEMPT ONE N=0
2 INDIC = ANALYSIS TYPE INDICATOR
1 NPRT = OUTPUT OPTIONS (1=MINIMUM, 2=MEDIUM, 3=MAXIMUM)
0 ISTRS = OUTPUT CONTROL (0=RESULTANTS, 1=SIGMA, 2=EPSILON)
3 NSEG = NUMBER OF SHELL SEGMENTS (LESS THAN 25)
H
H
10 SEGMENT NUMBER 1 1 1 1 1 1 1 1
3 NMESH = NUMBER OF NODE POINTS (5 = MIN.; 98 = MAX.)( 1)
1 NTYPE = CONTROL INTEGER (1 OR 2 OR 3) FOR NODAL POINT SPACING
0.0 NSHAPE = INDICATOR (1,2 OR 4) FOR GEOMETRY OF MERIDIAN
0.0 R1 = RADIUS AT BEGINNING OF SEGMENT (SEE P. 66)
16.81250 Z1 = AXIAL COORDINATE AT BEGINNING OF SEGMENT
0.0 R2 = RADIUS AT END OF SEGMENT
0.0 Z2 = AXIAL COORDINATE AT END OF SEGMENT
3 IMP = INDICATOR FOR IMPERFECTION (0=NONE, 1=SOME)
2.500000 NTYPEZ = CONTROL (1 OR 3) FOR REFERENCE SURFACE LOCATION
N ZVAL = DISTANCE FROM LEFTMOST SURF. TO REFERENCE SURF.
0 DO YOU WANT TO PRINT OUT R(S), R'(S), ETC. FOR THIS SEGMENT?
0.000000E+00 NRINGS = NUMBER (MAX=20) OF DISCRETE RINGS IN THIS SEGMENT
0 K=ELASTIC FOUNDATION MODULUS (E.G. LB/INCH3) IN THIS SEG.
0 LINTYP = INDICATOR (0, 1, 2 OR 3) FOR TYPE OF LINE LOADS
2 NLTYPE = CONTROL (0,1,2,3) FOR TYPE OF SURFACE LOADING
0.1080000E+08 NMALL = INDEX (1, 2, 4, 5, 6, 7, 8) FOR WALL CONSTRUCTION
0.3200000 E = YOUNG'S MODULUS FOR SKIN
0.2535000E-03 U = POISSON'S RATIO FOR SKIN
0.0000000E+00 SM = MASS DENSITY OF SKIN (E.G. ALUM.=.00025 LB-SEC2/INCH4)
0 ALPHA = COEFFICIENT OF THERMAL EXPANSION
1 ANRS = CONTROL (0 OR 1) FOR ADDITION OF SHEARED STIFFENERS
N SUR = CONTROL FOR THICKNESS INPUT (0 OR 1 OR -1)
H DO YOU WANT TO PRINT OUT THE C(I,J) AT MERIDIONAL STATIONS?
H DO YOU WANT TO PRINT OUT DISTRIBUTED LOADS ALONG MERIDIAN?
H
H
45 SEGMENT NUMBER 2 2 2 2 2 2 2 2
3 NMESH = NUMBER OF NODE POINTS (5 = MIN.; 98 = MAX.)( 2)
1 NTYPE = CONTROL INTEGER (1 OR 2 OR 3) FOR NODAL POINT SPACING
16.81250 NSHAPE = INDICATOR (1,2 OR 4) FOR GEOMETRY OF MERIDIAN
0.0000000E+00 R1 = RADIUS AT BEGINNING OF SEGMENT (SEE P. 66)
16.81250 Z1 = AXIAL COORDINATE AT BEGINNING OF SEGMENT
258.1250 R2 = RADIUS AT END OF SEGMENT
0 Z2 = AXIAL COORDINATE AT END OF SEGMENT
3 IMP = INDICATOR FOR IMPERFECTION (0=NONE, 1=SOME)
0.1875000 NTYPEZ = CONTROL (1 OR 3) FOR REFERENCE SURFACE LOCATION
N ZVAL = DISTANCE FROM LEFTMOST SURF. TO REFERENCE SURF.
6 DO YOU WANT TO PRINT OUT R(S), R'(S), ETC. FOR THIS SEGMENT?
2 NRINGS = NUMBER (MAX=20) OF DISCRETE RINGS IN THIS SEGMENT
3 NTYPE = CONTROL FOR IDENTIFICATION OF RING LOCATION (2=Z, 3=R)
3.500000 Z(I) = AXIAL COORDINATE OF ITH RING, Z( 1)
53.12500 Z(I) = AXIAL COORDINATE OF ITH RING, Z( 2)
103.7500 Z(I) = AXIAL COORDINATE OF ITH RING, Z( 3)
154.3750 Z(I) = AXIAL COORDINATE OF ITH RING, Z( 4)
205.0000 Z(I) = AXIAL COORDINATE OF ITH RING, Z( 5)
254.6250 Z(I) = AXIAL COORDINATE OF ITH RING, Z( 6)
1 NTYPE = TYPE (0 OR 1 OR 2 OR 4 OR 5) OF DISCRETE RING NO.( 1)
1 NTYPE = TYPE (0 OR 1 OR 2 OR 4 OR 5) OF DISCRETE RING NO.( 2)
1 NTYPE = TYPE (0 OR 1 OR 2 OR 4 OR 5) OF DISCRETE RING NO.( 3)
1 NTYPE = TYPE (0 OR 1 OR 2 OR 4 OR 5) OF DISCRETE RING NO.( 4)
1 NTYPE = TYPE (0 OR 1 OR 2 OR 4 OR 5) OF DISCRETE RING NO.( 5)
1 NTYPE = TYPE (0 OR 1 OR 2 OR 4 OR 5) OF DISCRETE RING NO.( 6)
0.3000000E+08 E = YOUNG'S MODULUS OF RING( 1)
7.125000 A = CROSS SECTION AREA OF RING( 1)
7.535500 IY = MOMENT OF INERTIA ABOUT Y-AXIS (SEE FIG. ON P.70)( 1)
2.375000 IX = MOMENT OF INERTIA ABOUT X-AXIS( 1)
0.0000000E+00 IXY = PRODUCT OF INERTIA( 1)
-1.781250 E1 = RADIAL COMPONENT OF RING ECCENTRICITY (SEE P. 70)( 1)
0.0000000E+00 E2 = AXIAL COMPONENT OF RING ECCENTRICITY( 1)
0.7501E+08 GJ = TORSIONAL RIGIDITY( 1)
0.7330000E-03 RM = RING MATERIAL DENSITY (E.G. ALUMINUM=.0002535)( 1)
0.3000000E+08 E = YOUNG'S MODULUS OF RING( 2)
8.250000 A = CROSS SECTION AREA OF RING( 2)
11.69800 IY = MOMENT OF INERTIA ABOUT Y-AXIS (SEE FIG. ON P.70)( 2)
2.750000 IX = MOMENT OF INERTIA ABOUT X-AXIS( 2)
0.0000000E+00 IXY = PRODUCT OF INERTIA( 2)

```

FILE: BOSSO DATA A1

```

-2.062500  * E1  = RADIAL COMPONENT OF RING ECCENTRICITY (SEE P. 70)( 2)
0.0000000E+00 * E2  = AXIAL COMPONENT OF RING ECCENTRICITY( 2)
0.9249000E+08 * GJ  = TORSIONAL RIGIDITY( 2)
0.7330000E-03 * RM  = RING MATERIAL DENSITY (E.G. ALUMINUM=.0002535)( 2)
0.3000000E+08 * E    = YOUNG'S MODULUS OF RING( 3)
8.250000    * A    = CROSS SECTION AREA OF RING( 3)
11.69800    * IY    = MOMENT OF INERTIA ABOUT Y-AXIS (SEE FIG. ON P.70)( 3)
2.750000    * IX    = MOMENT OF INERTIA ABOUT X-AXIS( 3)
0.0000000E+00 * IXY   = PRODUCT OF INERTIA( 3)
-2.062500    * E1    = RADIAL COMPONENT OF RING ECCENTRICITY (SEE P. 70)( 3)
0.0000000E+00 * E2    = AXIAL COMPONENT OF RING ECCENTRICITY( 3)
0.9249000E+08 * GJ    = TORSIONAL RIGIDITY( 3)
0.7330000E-03 * RM    = RING MATERIAL DENSITY (E.G. ALUMINUM=.0002535)( 3)
0.3000000E+08 * E      = YOUNG'S MODULUS OF RING( 4)
8.250000    * A      = CROSS SECTION AREA OF RING( 4)
11.69800    * IY      = MOMENT OF INERTIA ABOUT Y-AXIS (SEE FIG. ON P.70)( 4)
2.750000    * IX      = MOMENT OF INERTIA ABOUT X-AXIS( 4)
0.0000000E+00 * IXY     = PRODUCT OF INERTIA( 4)
-2.062500    * E1     = RADIAL COMPONENT OF RING ECCENTRICITY (SEE P. 70)( 4)
0.0000000E+00 * E2     = AXIAL COMPONENT OF RING ECCENTRICITY( 4)
0.9249000E+08 * GJ     = TORSIONAL RIGIDITY( 4)
0.7330000E-03 * RM     = RING MATERIAL DENSITY (E.G. ALUMINUM=.0002535)( 4)
0.3000000E+08 * E       = YOUNG'S MODULUS OF RING( 5)
8.250000    * A       = CROSS SECTION AREA OF RING( 5)
11.69800    * IY       = MOMENT OF INERTIA ABOUT Y-AXIS (SEE FIG. ON P.70)( 5)
2.750000    * IX       = MOMENT OF INERTIA ABOUT X-AXIS( 5)
0.0000000E+00 * IXY      = PRODUCT OF INERTIA( 5)
-2.062500    * E1      = RADIAL COMPONENT OF RING ECCENTRICITY (SEE P. 70)( 5)
0.0000000E+00 * E2      = AXIAL COMPONENT OF RING ECCENTRICITY( 5)
0.9249000E+08 * GJ      = TORSIONAL RIGIDITY( 5)
0.7330000E-03 * RM      = RING MATERIAL DENSITY (E.G. ALUMINUM=.0002535)( 5)
0.3000000E+08 * E        = YOUNG'S MODULUS OF RING( 6)
7.125000    * A        = CROSS SECTION AREA OF RING( 6)
7.535500    * IY        = MOMENT OF INERTIA ABOUT Y-AXIS (SEE FIG. ON P.70)( 6)
2.375000    * IX        = MOMENT OF INERTIA ABOUT X-AXIS( 6)
0.0000000E+00 * IXY       = PRODUCT OF INERTIA( 6)
-1.781250    * E1       = RADIAL COMPONENT OF RING ECCENTRICITY (SEE P. 70)( 6)
0.0000000E+00 * E2       = AXIAL COMPONENT OF RING ECCENTRICITY( 6)
0.7501E+08   * GJ       = TORSIONAL RIGIDITY( 6)
0.7330000E-03 * RM       = RING MATERIAL DENSITY (E.G. ALUMINUM=.0002535)( 6)
0.0000000E+00 * E        = K=ELASTIC FOUNDATION MODULUS (E.G. LB/IN**3) IN THIS SEG.
0              * LINTYP= INDICATOR (0, 1, 2 OR 3) FOR TYPE OF LINE LOADS
0              * NLTYPE=CONTROL (0,1,2,3) FOR TYPE OF SURFACE LOADING
2              * NMALL=INDEX (1, 2, 4, 5, 6, 7, 8) FOR WALL CONSTRUCTION
0.3000000E+08 * E        = YOUNG'S MODULUS FOR SKIN
0.3000000    * U        = POISSON'S RATIO FOR SKIN
0.7330000E-03 * SM=MAS* DENSITY OF SKIN (E.G. ALUM.=.00025 LB-SEC**2/IN**4)
0.0           * ALPHA = COEFFICIENT OF THERMAL EXPANSION
1             * ANRS = CONTROL (0 OR 1) FOR ADDITION OF SMEARED STIFFENERS
1             * SUR  = CONTROL FOR THICKNESS INPUT (0 OR 1 OR -1)
N             * ARE THERE STRINGERS (PLEASE ANSWER Y OR N)?
Y             * ARE THERE RINGS (PLEASE ANSWER Y OR N)?
0             * K2 =CONTROL (0 OR 1) FOR INTERNAL OR EXTERNAL RINGS
0.3000000E+08 * E2      = RING MODULUS
0.3000000    * U2      = RING POISSON RATIO
0.7330000E-03 * RGMDS= RING MASS DENSITY
Y             * IS THE RING CROSS SECTION CONSTANT IN THIS SEGMENT?
Y             * IS THE RING CROSS SECTION RECTANGULAR (Y OR N)?
5.625000    * D2      = ARC LENGTH BETWEEN ADJACENT RINGS (CONSTANT)
0.2500000    * T2      = THICKNESS OF RING (CONSTANT)
1.250000    * H2      = HEIGHT OF RING (CONSTANT)
N             * DO YOU WANT TO PRINT OUT THE C(I,J) AT MERIDIONAL STATIONS?
N             * DO YOU WANT TO PRINT OUT DISTRIBUTED LOADS ALONG MERIDIAN?
H            *
H            *
10           * SEGMENT NUMBER 3 3 3 3 3 3 3 3
3            * NMESH = NUMBER OF NODE POINTS (5 = MIN.; 98 = MAX.)( 3)
1            * NTYPE= CONTROL INTEGER (1 OR 2 OR 3) FOR NODAL POINT SPACING
16.81250    * NSHAPE= INDICATOR (1,2 OR 4) FOR GEOMETRY OF MERIDIAN
0.0          * R1      = RADIUS AT BEGINNING OF SEGMENT (SEE P. 66)
0.0000000E+00 * Z1     = AXIAL COORDINATE AT BEGINNING OF SEGMENT
0.0          * R2      = RADIUS AT END OF SEGMENT
0.0          * Z2      = AXIAL COORDINATE AT END OF SEGMENT

```

FILE: BOSSO DATA A1

```

0      * IMP = INDICATOR FOR IMPERFECTION (0=NONE, 1=SOME)
3      * NTYPEZ= CONTROL (1 OR 3) FOR REFERENCE SURFACE LOCATION
2.500000 * ZVAL = DISTANCE FROM LEFTMOST SURF. TO REFERENCE SURF.
N      * DO YOU WANT TO PRINT OUT R(S), R'(S), ETC. FOR THIS SEGMENT?
0      * NRINGS= NUMBER (MAX=20) OF DISCRETE RINGS IN THIS SEGMENT
0.0     * K=ELASTIC FOUNDATION MODULUS (E.G. LB/INCH3) IN THIS SEG.
0      * LINTYP= INDICATOR (0, 1, 2 OR 3) FOR TYPE OF LINE LOADS
0      * NLTYPE=CONTROL (0,1,2,3) FOR TYPE OF SURFACE LOADING
2      * NMALL=INDEX (1, 2, 4, 5, 6, 7, 8) FOR MALL CONSTRUCTION
0.1080000E+08 * E = YOUNG'S MODULUS FOR SKIN
0.3200000     * U = POISSON'S RATIO FOR SKIN
0.2535000E-03 * SM =MASS DENSITY OF SKIN (E.G. ALUM.=.00025 LB-SEC2/INCH4)
0.0          * ALPHA = COEFFICIENT OF THERMAL EXPANSION
0          * ANRS = CONTROL (0 OR 1) FOR ADDITION OF SMEARED STIFFENERS
1          * SUR = CONTROL FOR THICKNESS INPUT (0 OR 1 OR -1)
N          * DO YOU WANT TO PRINT OUT THE C(I,J) AT MERIDIONAL STATIONS?
N          * DO YOU WANT TO PRINT OUT DISTRIBUTED LOADS ALONG MERIDIAN?
H          *
H          * GLOBAL DATA...
-1         * NLAST = PLOT OPTIONS (-1=NONE, 0=GEOMETRY, 1=U,V,W)
0          * NOB = STARTING NUMBER OF CIRC. WAVES (BUCKLING ANALYSIS)
0          * NMIND = MINIMUM NUMBER OF CIRC. WAVES (BUCKLING ANALYSIS)
0          * NMAXB = MAXIMUM NUMBER OF CIRC. WAVES (BUCKLING ANALYSIS)
1          * INCRB = INCREMENT IN NUMBER OF CIRC. WAVES (BUCKLING)
30         * NVEC = NUMBER OF EIGENVALUES FOR EACH HAVE NUMBER
0.0000000E+00 * P = PRESSURE OR SURFACE TRACTION MULTIPLIER
0.0000000E+00 * TEMP = TEMPERATURE RISE MULTIPLIER
0.0000000E+00 * OMEGA = ANGULAR VEL. ABOUT AXIS OF REVOLUTION (RAD/SEC)
1          * NUMBER OF POLES (PLACES WHERE R=0) IN SEGMENT( 1)
H          *
H          * CONSTRAINT CONDITIONS FOR SEGMENT NO. 1 1 1 1
1          * IPOLE = NODAL POINT NUMBER OF POLE, IPOLE( 1)
0          * AT HOW MANY STATIONS IS THIS SEGMENT CONSTRAINED TO GROUND?
N          * IS THIS SEGMENT JOINED TO ANY LOWER-NUMBERED SEGMENTS?
0          * NUMBER OF POLES (PLACES WHERE R=0) IN SEGMENT( 2)
H          *
H          * CONSTRAINT CONDITIONS FOR SEGMENT NO. 2 2 2 2
0          * AT HOW MANY STATIONS IS THIS SEGMENT CONSTRAINED TO GROUND?
Y          * IS THIS SEGMENT JOINED TO ANY LOWER-NUMBERED SEGMENTS?
1          * AT HOW MAY STATIONS IS THIS SEGMENT JOINED TO PREVIOUS SEGS.?
1          * INODE = NODE IN CURRENT SEGMENT (ISEG) OF JUNCTION, INODE( 1)
1          * JSEG = SEGMENT NO. OF PREVIOUS SEGMENT INVOLVED IN JUNCTION
10         * JNODE = NODE IN PREVIOUS SEGMENT (JSEG) OF JUNCTION
1          * IUSTAR= AXIAL DISPLACEMENT (0=NOT SLAVED, 1=SLAVED)
1          * IVSTAR= CIRCUMFERENTIAL DISPLACEMENT (0=NOT SLAVED, 1=SLAVED)
1          * IMSTAR= RADIAL DISPLACEMENT (0=NOT SLAVED, 1=SLAVED)
1          * ICHI = MERIDIONAL ROTATION (0=NOT SLAVED, 1=SLAVED)
0.0000000E+00 * D1 = RADIAL COMPONENT OF JUNCTURE GAP
0.0000000E+00 * D2 = AXIAL COMPONENT OF JUNCTURE GAP
Y          * IS THIS CONSTRAINT THE SAME FOR BOTH PREBUCKLING AND BUCKLING?
1          * NUMBER OF POLES (PLACES WHERE R=0) IN SEGMENT( 3)
H          *
H          * CONSTRAINT CONDITIONS FOR SEGMENT NO. 3 3 3 3
10         * IPOLE = NODAL POINT NUMBER OF POLE, IPOLE( 1)
0          * AT HOW MANY STATIONS IS THIS SEGMENT CONSTRAINED TO GROUND?
Y          * IS THIS SEGMENT JOINED TO ANY LOWER-NUMBERED SEGMENTS?
1          * AT HOW MAY STATIONS IS THIS SEGMENT JOINED TO PREVIOUS SEGS.?
1          * INODE = NODE IN CURRENT SEGMENT (ISEG) OF JUNCTION, INODE( 1)
2          * JSEG = SEGMENT NO. OF PREVIOUS SEGMENT INVOLVED IN JUNCTION
45         * JNODE = NODE IN PREVIOUS SEGMENT (JSEG) OF JUNCTION
1          * IUSTAR= AXIAL DISPLACEMENT (0=NOT SLAVED, 1=SLAVED)
1          * IVSTAR= CIRCUMFERENTIAL DISPLACEMENT (0=NOT SLAVED, 1=SLAVED)
1          * IMSTAR= RADIAL DISPLACEMENT (0=NOT SLAVED, 1=SLAVED)
1          * ICHI = MERIDIONAL ROTATION (0=NOT SLAVED, 1=SLAVED)
0.0000000E+00 * D1 = RADIAL COMPONENT OF JUNCTURE GAP
0.0000000E+00 * D2 = AXIAL COMPONENT OF JUNCTURE GAP
Y          * IS THIS CONSTRAINT THE SAME FOR BOTH PREBUCKLING AND BUCKLING?
Y          * DO YOU WANT TO LIST OUTPUT FOR SEGMENT( 1)
Y          * DO YOU WANT TO LIST OUTPUT FOR SEGMENT( 2)
Y          * DO YOU WANT TO LIST OUTPUT FOR SEGMENT( 3)
N          * DO YOU WANT TO LIST PREBUCKLING RESULTANTS AND RING FORCES?

```

2. ACESNID INPUT DATA

The ACESNID computer code determines the virtual mass array, a quantity producing the late-time contribution of the DAA. Only one ACESNID calculation is required for all circumferential harmonics of the shell. The bands dividing the areas of the shell are identified in the NLEFT, NCYL, and NRITE entries, while the fluid properties are specified in the RHOFL and VSOUND row.

FILE: ACE1 DATA A1

VIRTUAL MASS FOR RING-STIFFENED CYLINDER WITH FLAT ENDS, N=0,1
0 1 1 1 0 / NSTART,NFINIS,NFREQ,NVMASS,NCHECK
15 51 15 3 0 / NLEFT,NCYL,NRITE,NWBOSG,NSYMF
1 6 10 0 0 / NORDER,NFENDS,NFCENT,NFCMPT,NOMIT
9.59684E-5 5.833E4 0.005 / RHOFL,VSOUND,ERR
1 1 1 1 1 0 1 1 1 / OUTPUT FLAGS
1.0 / CPS(1)
1 1 1 12 / SEFS,JSGBEG,JPTBEG,JSGEND,JPTEND,LEFT
2 1 2 47 / SEFS,JSGBEG,JPTBEG,JSGEND,JPTEND,CENTRAL
3 1 3 12 / SEFS,JSGBEG,JPTBEG,JSGEND,JPTEND,RIGHT
1 1 1 12 / SOURCES,JSGBEG,JPTBEG,JSGEND,JPTEND,LEFT
2 1 2 47 / SOURCES,JSGBEG,JPTBEG,JSGEND,JPTEND,CENTRAL

3. PIFLASH INPUT DATA

The PIFLASH code takes data from the shell mode files from BOSOR4 and the virtual mass file from ACESNID and combines them to create a "shell-fluid file" containing all the information concerning the shell and its acoustic medium for further calculations. Since only the breathing modes are activated in end-on loading, all torsional modes are dropped from the shell file. This is accomplished in the NJUSE rows where the modes of Table I are identified.

FILE: PIE1 DATA A1

```
2 0 0 0 0 / NUMBER, NTORSN, NPTM, NSYMS, NSYMP
3 3 3 3 / (NWETSG(K), NUESG(K), K=1, 2)
386.4 / GRAVITY
SHELL00 / SMF, N=0
SHELL01 / SMF, N=1
19 2 / (NJUSE(J), J=1, NITEMS)
1 2 3 / (KORSG(K), K=1, NKORSG)
2 4 6 7 9 12 13 14 19 20 21 22 23 25 26 27 28 29 30 / JUSE, N=0
1 2 / JUSE, N=1
```

4. SAPIV INPUT DATA

The substructure is modeled using the standard SAPIV code with slight modifications by the developers of ELSHOK. The diaphragm is modeled using twenty-four plates and twenty-five nodes. The location of each node is identified in cartesian coordinates. Each plate is 1.06 in thick for the resonant case. Nodes eighteen through twenty-five are rigidly attached to the shell in the last eight lines of the code. The SAPIV code determines the fixed-base modes and corresponding natural frequencies as well as the unconstrained mass and stiffness matrices for the substructure.

FILE: SAP23 DATA A1

IDEALIZED INTERNAL EQUIPMENT AT FRAME 9
25 1 0 10 1 0 0 0 0 0 / NUMNP,NELTYP,....,N10SV,NRIGID
0 1 0 1 1 1 1 1 0.0 0.0 0.0 0.0
0 2 0 0 0 1 0 0 0.0 0.0 5.604 0 0.0
0 3 0 0 0 1 0 0 0.0 3.963 3.963 0 0.0
0 4 0 0 0 1 0 0 0.0 5.604 0.0 0 0.0
0 5 0 0 0 1 0 0 0.0 3.963 -3.963 0 0.0
0 6 0 0 0 1 0 0 0.0 0.0 -5.604 0 0.0
0 7 0 0 0 1 0 0 0.0 -3.963 -3.963 0 0.0
0 8 0 0 0 1 0 0 0.0 -5.604 0.0 0 0.0
0 9 0 0 0 1 0 0 0.0 -3.963 3.963 0 0.0
0 10 0 0 0 1 0 0 0.0 0.0 11.208 0 0.0
0 11 0 0 0 1 0 0 0.0 7.925 7.925 0 0.0
0 12 0 0 0 1 0 0 0.0 11.208 0.0 0 0.0
0 13 0 0 0 1 0 0 0.0 7.925 -7.925 0 0.0
0 14 0 0 0 1 0 0 0.0 0.0 -11.208 0 0.0
0 15 0 0 0 1 0 0 0.0 -7.925 -7.925 0 0.0
0 16 0 0 0 1 0 0 0.0 -11.208 0.0 0 0.0
0 17 0 0 0 1 0 0 0.0 -7.925 7.925 0 0.0
0 18 0 0 0 1 0 0 0.0 0.0 16.813 0 0.0
0 19 0 0 0 1 0 0 0.0 11.888 11.888 0 0.0
0 20 0 0 0 1 0 0 0.0 16.813 0.0 0 0.0
0 21 0 0 0 1 0 0 0.0 11.888 -11.888 0 0.0
0 22 0 0 0 1 0 0 0.0 0.0 -16.813 0 0.0
0 23 0 0 0 1 0 0 0.0 -11.888 -11.888 0 0.0
0 24 0 0 0 1 0 0 0.0 -16.813 0.0 0 0.0
0 25 0 0 0 1 0 0 0.0 -11.888 11.888 0 0.0
6 24 1 / TYPE 6 (PLATE AND SHELL ELEMENTS)
1 .733E-03 0.0 0.0 0.0
32.967E+06 9.89E+06 0.0 32.967E+06 0.0 11.538E+06
0.0 0.0 0.0 0.0
0.0 0.0 0.0 0.0
0.0 0.0 0.0 0.0
0.0 0.0 0.0 0.0
0.0 0.0 0.0 0.0 / ELEMENT LOAD MULTIPLIERS
1 1 8 9 0 0 1 0 1.06 0 0 0
2 1 9 2 0 0 1 0 1.06 0 0 0
3 1 2 3 0 0 1 0 1.06 0 0 0
4 1 3 4 0 0 1 0 1.06 0 0 0
5 1 4 5 0 0 1 0 1.06 0 0 0
6 1 5 6 0 0 1 0 1.06 0 0 0
7 1 6 7 0 0 1 0 1.06 0 0 0
8 1 7 8 0 0 1 0 1.06 0 0 0
9 2 10 11 3 0 1 1 1.06 0 0 0
15 8 16 17 9 0 1 0 1.06 0 0 0
16 9 17 10 2 0 1 0 1.06 0 0 0
17 10 18 19 11 0 1 1 1.06 0 0 0
23 16 24 25 17 0 1 0 1.06 0 0 0
24 17 25 18 10 0 1 0 1.06 0 0 0
0 0 0.0 0.0 0.0 0.0 0.0 0.0 0.0 / CONC MASSES
0.0 0.0 0.0 0.0 / ELEMENT LOAD MULTIPLIERS
0 0 0 0.0 0.0 0.0 / IFPR,IFSS,....,NFO,SHIFT
8 0 / NFACE,NSYMTY
18 1 1 1 1 0 0
19 1 1 1 1 0 0
20 1 1 1 1 0 0
21 1 1 1 1 0 0
22 1 1 1 1 0 0
23 1 1 1 1 0 0
24 1 1 1 1 0 0
25 1 1 1 1 0 0
END OF DATA (DUMMY TITLE)

5. PICRUST INPUT DATA

The PICRUST code takes data from the substructure mode file from SAPIV and reorganizes it to facilitate the solution of the transient response equations. The location of the substructure attachment points to the shell is identified for each connecting node.

FILE: PICRUST1 DATA A1

```
1 1 1 1 0 1 1 1 0 0
0 1 1 1 1 1 0 1 0 1 / OUTPUT FLAGS 1-20
2 0 0 / NJUSE,NHWSOB,NHWBAR
18 2 11 0.0
19 2 11 45.0
20 2 11 90.0
21 2 11 135.0
22 2 11 180.0
23 2 11 225.0
24 2 11 270.0
25 2 11 315.0 / NIPSUB,LBOSEG,LBOSPT,ANGDEG
0.0 / DEGROT
```

6. USLOB INPUT DATA

The two USLOB input codes for the taper and conventional charges appear on the following page. USL46 DATA is the code for the taper charge. It contains nine discrete data points from the pressure-time history in seconds and pounds per square inch. There are 1600 time points used in the numerical integration of the governing equations with information saved every sixteenth point, so only 100 velocity-time data points are retained for EASYPLOT display. The charge is placed along the negative X-axis at 840 inches. USL47 DATA contains the information for the conventional charge. The only difference between the two codes is a charge identification entry (NCHRG) and the charge weight and constants specified for the conventional charge instead of the pressure-time history (WCHRG-THEXP).

FILE: USL46 DATA A1

1599 16 2 9 2 2 1 / NTIME,NSKIP,NCHRG,NQUAD,NFINE,KOUPLE,NSUBS
5.0E-05 -840.0 0.0 0.0 / DELT,XLOAD,RLOAD,SURCUT
9 / NSHAPE
0.0 240.0 0.0002 320.0 0.00053 350.0 0.00243 305.0 0.00294 160.0
0.0034 115.0 0.0044 70.0 0.0054 48.0 0.00565 0.0 / (TC(J),PC(J),J=1,NSHAPE)
0.0 / DECAY
0 1 0 0 0 0 0 0 0
0 0 1 0 0 0 0 0 0 / OUTPUT FLAGS 1-20
4 / NPTSHL
1 1 2 11 2 46 3 12 / LBOSEG,LBOSPT
1 / NPTSUB

FILE: USL47 DATA A1

1599 16 1 9 2 2 1 / NTIME,NSKIP,NCHRG,NQUAD,NFINE,KOUPLE,NSUBS
5.0E-05 -840.0 0.0 0.0 / DELT,XLOAD,RLOAD,SURCUT
352.0 3.8354314E+5 1.144 3.03131E-5 -.247 / WCHRG,PZMLT,PZEXP,THMLT,THEXP
0 1 0 0 0 0 0 0 0
0 0 1 0 0 0 0 0 0 / OUTPUT FLAGS 1-20
4 / NPTSHL
1 1 2 11 2 46 3 12 / LBOSEG,LBOSPT
1 / NPTSUB

7. PUSLOB INPUT DATA

The PUSLOB code produces TEKTRONIX plots of the velocity-time histories for specified points on the shell or substructure. It also generates velocity punch card files which are converted to a format for EASYPLOT using the PLOTCONV1 code.

FILE: PUSL46 DATA A1

1599 16 1 1 1 / NTIME,NSKIP,NSUBS,NTEK,NCARD
5.0E-05 1000.0 1.0 / DELT,XMULT,YMULT

VELOCITY PROFILE

TIME (MSEC)

VELOCITY (IN/SEC)

2 NPTSHL-W

V-FWD 1/01

1 1 -1 1 0.0

V-FWD 3/12

3 12 -1 1 0.0 / LBOSEG,LBOSPT,NSPHC,NANG,ANGDEG

13 NPTSHL-U

V-FWD 1/01

1 1 1 1 0.0

V-FWD 2/02

2 2 0 1 0.0

V-FWD 2/07

2 7 0 1 0.0

V-FWD 2/11

2 11 0 1 0.0

V-FWD 2/15

2 15 0 1 0.0

V-FWD 2/20

2 20 0 1 0.0

V-FWD 2/24

2 24 0 1 0.0

V-FWD 2/28

2 28 0 1 0.0

V-FWD 2/33

2 33 0 1 0.0

V-FWD 2/37

2 37 0 1 0.0

V-FWD 2/41

2 41 0 1 0.0

V-FWD 2/46

2 46 0 1 0.0

V-FWD 3/12

3 12 1 1 0.0 / LBOSEG,LBOSPT,NSPHC,NANG,ANGDEG

2 NPTSHL-V

V-FWD 1/01

1 1 -1 1 0.0

V-FWD 3/12

3 12 -1 1 0.0 / LBOSEG,LBOSPT,NSPHC,NANG,ANGDEG

1 NPTSUB

PLT CNTR

INITIAL DISTRIBUTION LIST

	<u>No. Copies</u>
1. Defense Technical Information Center Cameron Station Alexandria, Virginia 22304-6145	2
2. Library, Code 0142 Naval Postgraduate School Monterey, California 93943-5002	2
3. Professor Y. S. Shin, Code 69Sg Department of Mechanical Engineering Naval Postgraduate School Monterey, California 93943-5000	5
4. Professor R. E. Newton, Code 69Ne Department of Mechanical Engineering Naval Postgraduate School Monterey, California 93943-5000	1
5. Department Chairman, Code 69 Department of Mechanical Engineering Naval Postgraduate School Monterey, California 93943-5000	1
6. Dr. N. T. Tsai Defense Nuclear Agency SPSS Washington, D.C. 20305-1000	3
7. Dr. E. Sevin Defense Nuclear Agency Washington, D.C. 20305-1000	1
8. Dr. M. L. Baron Weidlinger Associates 333 Seventh Avenue New York, NY 10001	1
9. Dr. Ranlet Weidlinger Associates 333 Seventh Avenue New York, NY 10001	1

- | | | |
|-----|---|---|
| 10. | Dr. Andrew P. Misovec
5202 W. Military Hwy
Chesapeake, Virginia 23321 | 1 |
| 11. | Dr. B. Whang, Code 1750.2
Hull Group Head, Submarine Protection Div.
David Taylor Naval Ship Research
and Development Center
Bethesda, Maryland 20084 | 1 |
| 12. | Dr. Huang, Code R14
Naval Surface Weapon Center
White Oaks
Silver Spring, Maryland 20910 | 1 |
| 13. | LCDR S. A. Weinhardt, USN
6611 Belmead Drive
Dallas, Texas 75230 | 2 |
| 14. | W. T. Weinhardt
6611 Belmead Drive
Dallas, Texas 75230 | 1 |
| 15. | LT N. Williams, USN
125 Surf Way, Apt. 438
Monterey, California 93940 | 1 |

END

DTIC

6-86